# TWO LINKS AT ONE POINT: AN ILLUSTRATED COMPANION TO THE CONSTRUCTION

ANASS NIFA

Abstract. This companion explains the construction in *Topological singularities in the codimension-two stratum of noncollapsed Ricci limits*. The fixed manifold recording the topology of a punctured neighbourhood differs from the limiting link determining its metric tangent. We follow this distinction through the actual edge regularization, the construction of caps with prescribed boundary tensors, the uniform parameter choices, and the two volume normalizations. We then explain the radial curvature estimates, the comparison of ambient distances, and the exact smooth filling procedure. The local homology calculation identifies the obstruction to a manifold chart, although the neighbourhood is contractible and the unique metric tangent is topologically Euclidean.

## 1. The statement, with dimensions visible

*Start with the objects; keep the two cone constructions separate.*

Fix $n \geq 4$ and a closed connected oriented smooth manifold $Q^n$. Put $N = n+1$, $\sigma_k = \mathrm{Vol}(S^k)$ and $\omega_k = \mathrm{Vol}(B_1^{\mathbb{R}^k})$, so that $\sigma_n = (n+1)\omega_{n+1}$. Homology is singular homology. Its coefficient group $A$ is an arbitrary abelian group unless specified.

| Object | Dimension | Role |
|---|---|---|
| $Q$, $P_Q$ | $n$ | Core manifold; $P_Q = Q \setminus \operatorname{int} D_Q$ |
| $M_Q = Q\#(-Q)$ | $n$ | Fixed smooth link of the radial product |
| $B_{n,q}$ | $n-1$ | Limit of sphere metrics $h_s$ |
| $L_{n,q} = S^0 * B_{n,q}$ | $n$ | Link of the unique metric tangent |
| $Y$ and $\mathrm{C}(L_{n,q})$ | $N = n+1$ | Completed space and its tangent |

The input is *core-admissibility*. There are a smoothly embedded closed disc $D_Q \subset Q$, a fixed boundary identification $\beta_Q : S^{n-1} \to \partial P_Q$, and a metric $k_Q$ such that

$$\beta_Q^*(k_Q|_{\partial P_Q}) = g_{S^{n-1}}, \qquad \beta_Q^* \mathrm{II}_{\partial P_Q, k_Q} \geq \kappa_Q g_{S^{n-1}}, \qquad \mathrm{Ric}_{k_Q} \geq \mu_Q k_Q$$

for constants $\kappa_Q, \mu_Q > 0$. Throughout this companion the inward unit normal $\nu$ defines

$$\mathrm{II}(v, w) = -\langle \nabla_v \nu, w \rangle.$$

All boundary comparisons use the specified pullback. Write $\bar{\kappa}_Q = \min\{1, \kappa_Q\}$. The boundary sphere is connected, and a component of $P_Q$ disjoint from that boundary would be open and closed in $Q$; thus $P_Q$ is connected. [N, Definition 3.1].

**The construction.** For each such $Q$, there is $q_0 = q_0(n, Q) > 0$, which may be decreased to be less than $1/2$, such that every $0 < q < q_0$ admits a complete pointed classical noncollapsed Ricci limit $(Y^N, d, p)$ with

$$\mathrm{Tan}(Y, p) = \{\mathbb{R}^{n-1} \times \mathrm{C}(S^1_{2\pi q})\},$$
$$(B_{r_0}(p), p) \cong (\mathrm{C}_{\mathrm{top}, r_0}(M_Q), o),$$
$$Y \setminus \{p\} \cong (0, \infty) \times M_Q.$$

The last identification is smooth. The realizing manifolds are complete, connected, smooth and without boundary, have nonnegative Ricci curvature, and have a common positive lower bound for the volumes of their based unit balls. Moreover,

$$H_j(Y, Y \setminus \{p\}; A) \cong \widetilde{H}_{j-1}(M_Q; A) \quad (j \geq 0), \qquad \Theta^N(Y, p) = q, \qquad \partial_{\mathrm{KM}} Y = \emptyset.$$

Here $\widetilde{H}_{-1}(M_Q; A) = 0$. If $M_Q$ is not an integral homology $n$-sphere, then $p$ has no manifold neighbourhood. These are the conclusions of [N, Theorem 3.2]; the boundary is specifically the Kapovitch–Mondino boundary.

Neither closed realizing manifolds nor a uniform strictly positive Ricci bound on the entire realizing manifolds is asserted here.

The notation $\mathrm{C}_{\mathrm{top},r_0}(M) = ([0, r_0) \times M)/(\{0\} \times M)$ means an open truncated *topological* cone. Its occurrence above is a homeomorphism, not an isometry to a fixed cone metric on $M_Q$. In contrast, the metric cone has distance

$$d_{\mathrm{C}(L)}([r, x], [s, y])^2 = r^2 + s^2 - 2rs\cos(\min\{d_L(x, y), \pi\}).$$

Its link is obtained after a metric limit. The fixed manifold $M_Q$ records the topology before that limit.

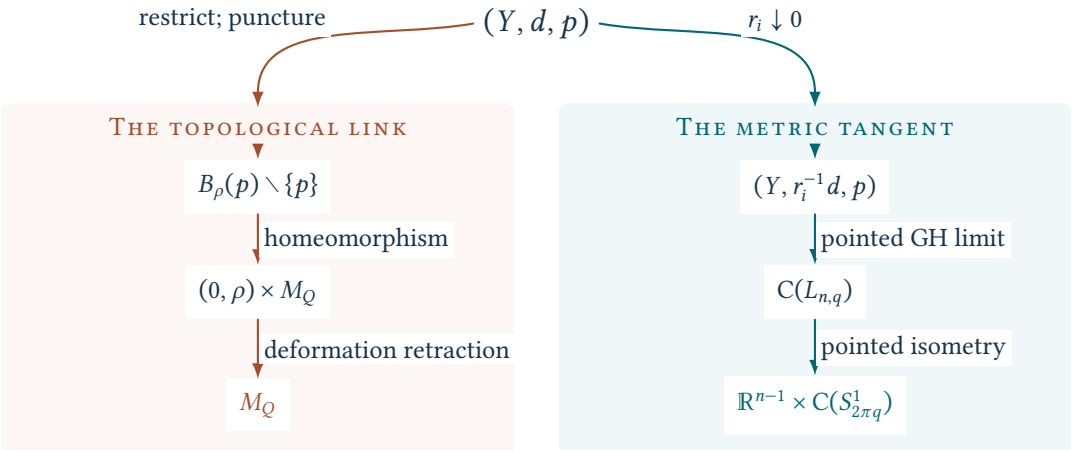



FIGURE 1. Two operations at the same point. Puncturing a small neighbourhood gives $(0, \rho) \times M_Q$ and its retraction onto $M_Q$. Rescaling and passing to the metric limit gives $\mathrm{C}(L_{n,q})$. These are two kinds of link, not two different metric tangent cones.

## 2. A map of the proof

*Three construction stages, followed by two readings of the same space.*

The first stage constructs sphere metrics $h_s$ and caps that replace the poles of their suspensions by punctured copies of $Q$. The second produces a family on one fixed $M_Q$, normalizes its Ricci bound and volume form, and retains a closable initial metric. The third places this family at shrinking radii, completes the punctured space, and realizes the completion by smooth manifolds. [N, §4, Theorem 8.1 and Proposition 9.2].

*The obstruction before the estimates.* Take $n = 4$, $Q = \mathbb{CP}^2$ and $U = B_{r_0}(p)$. The topological cone contracts by $[r, x] \mapsto [(1-t)r, x]$, while $U \setminus \{p\}$ retracts onto $M_Q$. The disc-removal and connected-sum exact sequences give $H_2(M_Q; \mathbb{Z}) = \mathbb{Z}^2$. Therefore

$$H_2(U; \mathbb{Z}) = 0, \qquad H_2(U \setminus \{p\}; \mathbb{Z}) = \mathbb{Z}^2, \qquad H_3(Y, Y \setminus \{p\}; \mathbb{Z}) = \mathbb{Z}^2.$$

The last group is incompatible with the local homology of a manifold point. Smaller conical neighbourhoods form a basis and are contractible. Thus the obstruction is not failure of local contractibility: it is the homology of the pair consisting of a neighbourhood and its puncture. Section 21 gives the exact-sequence argument. [N, Corollary 3.3 and §10].

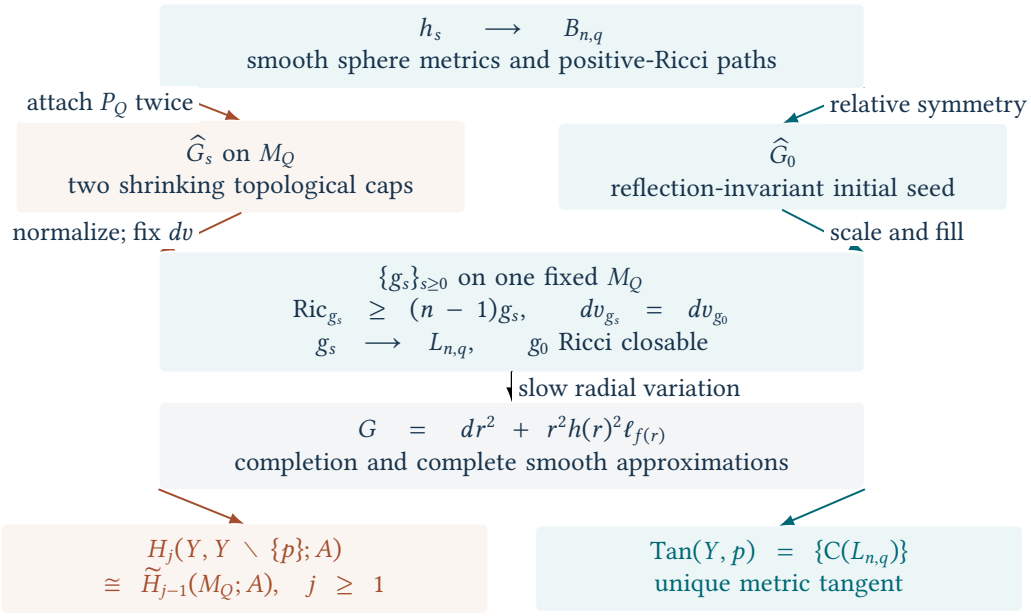



FIGURE 2. The construction and its dependencies. Degenerating sphere links and a reflection-symmetric initial seed enter the same normalized family. Radial realization yields a topological-cone neighbourhood and a unique metric tangent. The displayed local-homology formula for $j \geq 1$ extends to $j = 0$ by the convention in Section 1.

| Reading | Companion sections and key pictures | Main manuscript |
|---|---|---|
| Conceptual | 1–3, 14–15, 21–22<br>*Key pictures:* Figures 1, 27, 29; Visual A | §4; Theorems 3.2, 8.1; Proposition 9.2 |
| Constructing the links | 5, 6, 8–11<br>*Key pictures:* Visuals B, F, G, K | §§5–8 |
| Radial geometry | 12–20<br>*Key pictures:* Visuals O, P, S, U | Proposition 6.2; §9 |

Figures organize the construction and its worked models; Visuals provide complementary close-ups of particular identities, parameter choices and proof steps. The surface and scalar-model plots are illustrations of their displayed formulas. They are not substitutes for the higher-dimensional curvature estimates. A first reading may pass directly from each construction's inputs to its outputs.

*What is specific to this construction.* The comparison in [N, §1] distinguishes earlier phenomena from the combination proved here. Menguy's examples already show that topologically Euclidean tangents do not force a manifold neighbourhood; Colding–Naber construct variation among tangents, and Reiser prescribes collections of cross-sections. Here the asserted combination is a unique, explicitly identified tangent with maximal Euclidean factor of dimension $N-2$, an isolated nonmanifold point, a conical neighbourhood with computable local homology, and an empty prescribed codimension-four stratum. Merely saying that topology disappears in a tangent would not describe the full distinction made in the manuscript.

## 3. THE LIMITING METRIC LINK

*A short circle changes the metric without changing the topology of the join.*

For $0 < q < 1$, the intrinsic circle $S^1_{2\pi q}$ has diameter $\pi q$. Set

$$B_{n,q} = S^{n-3} * S^1_{2\pi q}, \qquad L_{n,q} = S^{n-2} * S^1_{2\pi q} = S^0 * B_{n,q}.$$

On the open join stratum,

$$g_L = d\theta^2 + \cos^2\theta\, g_{S^{n-2}} + q^2 \sin^2\theta\, d\phi^2, \quad 0 < \theta < \pi/2, \quad \phi \in \mathbb{R}/(2\pi\mathbb{Z}). \tag{3.1}$$

At $\theta = 0$ the circle collapses; at $\theta = \pi/2$ the sphere collapses. The first locus is the metric edge. The quotient map

$$[\theta, x, \phi] \longmapsto (\cos\theta\, x, \sin\theta\cos\phi, \sin\theta\sin\phi)$$

is a continuous bijection from the compact join quotient onto $S^n$, hence a homeomorphism. It is not generally an isometry. [N, Lemma 5.1].

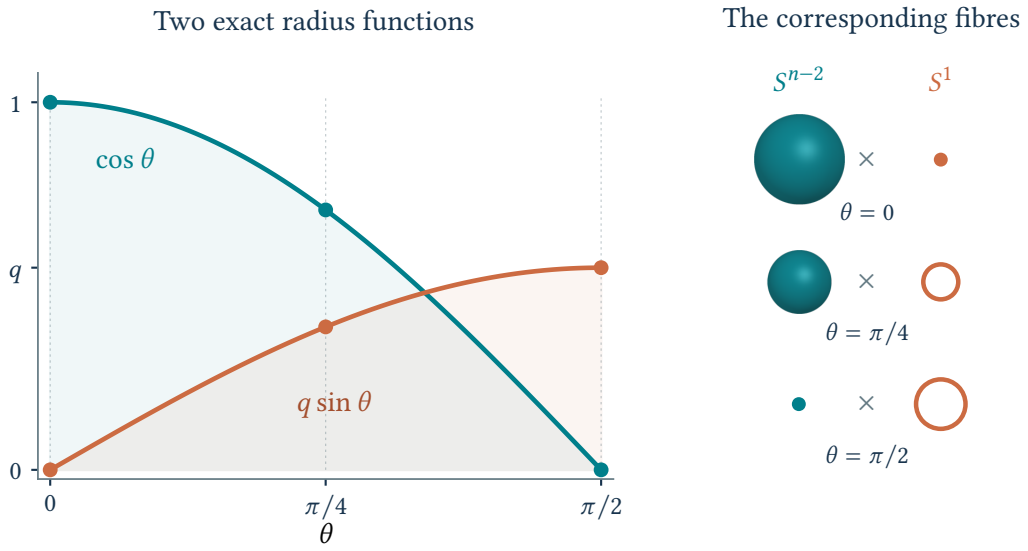



FIGURE 3. The exact radius functions $\cos\theta$ and $q\sin\theta$, and their product-factor symbols. The circle collapses at the metric edge; the sphere collapses smoothly at the other endpoint. The displayed $q = 0.55$ illustrates the join formulas, not the smallness threshold of the full construction.

The volume density on the regular stratum is $q$ times the round density. The two endpoint strata have zero $n$-dimensional measure, so

$$\mathcal{H}^n(L_{n,q}) = q\sigma_n.$$

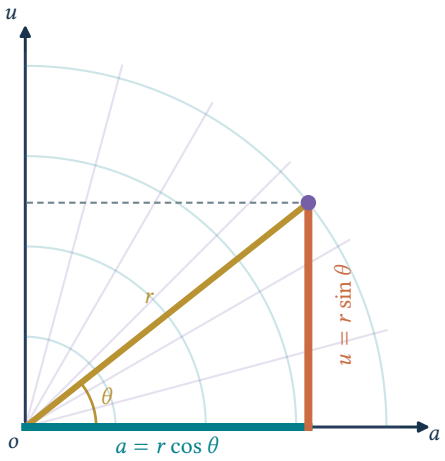
The cone–join map separates the two radial factors:

$$[r, [\theta, x, \phi]] \longmapsto ([r\cos\theta, x], [r\sin\theta, \phi]).$$

The cone and join distance formulas show that it is a pointed isometry. Consequently

$$\mathrm{C}(L_{n,q}) \cong_{\mathrm{iso}} \mathbb{R}^{n-1} \times \mathrm{C}(S^1_{2\pi q}). \tag{3.2}$$

The underlying space is $\mathbb{R}^{n+1}$; the cone-angle defect is metric, not topological. [N, Lemma 5.1].




$$dr^2 + r^2 d\theta^2 = da^2 + du^2$$

$$da^2 + a^2 g_{S^{n-2}}$$

$$\mathbb{R}^{n-1}$$

$$du^2 + q^2 u^2 d\phi^2$$

$$C(S^1_{2\pi q})$$

$$r^2 = a^2 + u^2$$

VISUAL A. The cone–join isometry in radial coordinates. The quadrant is the exact change of variables $a = r\cos\theta$, $u = r\sin\theta$: the radial tensor becomes $da^2 + du^2$, and the two fibre terms become the Euclidean polar factor and the circle-cone factor. This is a coordinate diagram; the missing sphere and circle variables remain independent.

## 4. A GEOMETRIC PICTURE OF THE CIRCLE CONE

*The only non-Euclidean factor is two-dimensional.*

Pair the two rays of a Euclidean sector of angle $2\pi q$ at equal radii. Its quotient length tensor is $du^2 + q^2u^2d\phi^2$. For $0 < q < 1$, the surface

$$F(u, \phi) = (qu\cos\phi, qu\sin\phi, \sqrt{1 - q^2}\, u)$$

has exactly that tensor: $|F_u|^2 = 1$, $|F_\phi|^2 = q^2u^2$ and $\langle F_u, F_\phi\rangle = 0$. The relevant distance is the intrinsic surface length distance, not Euclidean chord distance. The product tangent has metric singular axis $\mathbb{R}^{N-2} \times \{o\}$ but is topologically $\mathbb{R}^N$. The original nonmanifold examples are smooth away from one point. These statements concern different metric spaces; passage to a blow-up does not require convergence of their singular sets as subsets. The precise splitting argument is given in Section 22.

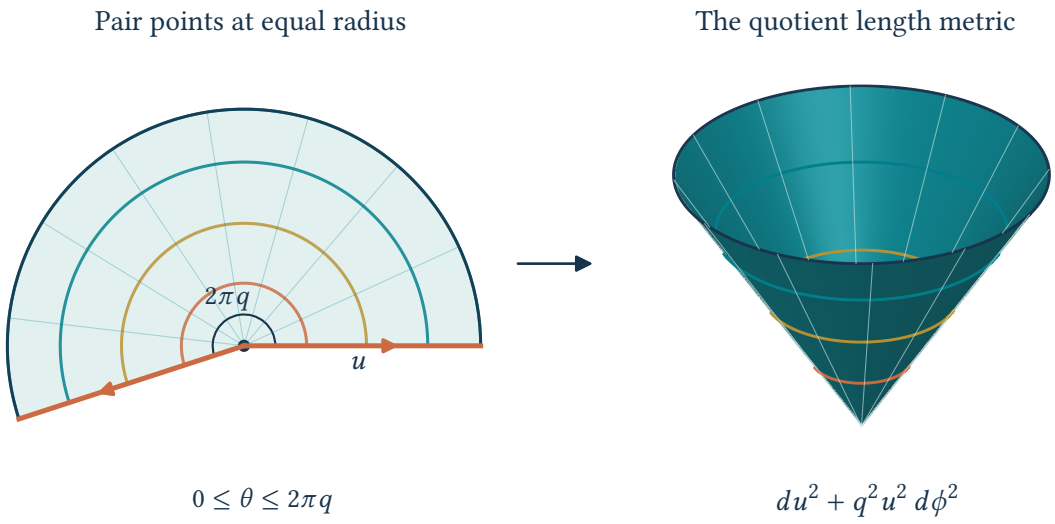



FIGURE 4. Pairing the radial edges of the sector gives the exact cone surface with its intrinsic length metric. Equal colours indicate equal intrinsic radii. The value $q = 0.55$ is illustrative and independent of the full construction's threshold.

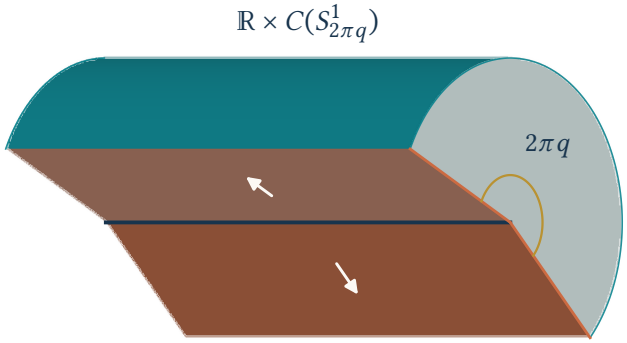



FIGURE 5. A fundamental domain for $\mathbb{R} \times C(S^1_{2\pi q})$, with the two radial faces paired at equal coordinates. The full tangent contains $N - 2$ Euclidean directions; the end faces are only truncations of the display.

## 5. SMOOTHING THE EDGE WHILE KEEPING A SURPLUS

*Construct the sphere path, not merely its limiting picture.*

The required sphere metrics satisfy

$$\mathrm{Ric}_{h_s} \ge (n-2)h_s, \qquad \mathrm{Vol}(h_s) = \gamma(s)\sigma_{n-1}, \qquad (S^{n-1}, h_s) \xrightarrow[s\to\infty]{\mathrm{GH}} B_{n,q}, \tag{5.1}$$

where $\gamma(s) > q$, $\gamma(s) \downarrow q$, and the initial metric is round. First fix $\gamma_* \in (0,1)$ with $\gamma_*^{1/(n-1)} < \bar{\kappa}_Q/4$; the final admissible $q$ is chosen below $\gamma_*$. For each $s$, the cap requires a path from $\tau_s^2 g_{S^{n-1}}$ to $h_s$, with $\tau_s = \gamma(s)^{1/(n-1)}$, constant near its two endpoints, of constant total volume in the path parameter, and with the same Ricci lower bound. We explain how these requirements are made compatible. [N, Lemma 5.2 and Theorem 5.3].

**The actual higher-dimensional profile.** Put $m = n - 1 \geq 3$. To distinguish the edge angle from the later relative volume excess, write $\beta_e$ for the parameter denoted $\beta$ in [N, Lemma 5.2]. For $q \leq \beta_e \leq 1$ and $0 < A < 1$, the raw metric is

$$g^{\mathrm{raw}}_{A,\beta_e} = A^2\big(dt^2 + \cos^2 t\, g_{S^{m-2}} + \beta_e^2 \sin^2 t\, d\theta^2\big).$$

Choose a smooth nondecreasing $\chi : [0,\infty) \to [0,1]$ equal to zero on $[0,1/2]$ and one on $[1,\infty)$. Define

$$J(\rho) = \int_0^{\pi/2} \chi(t/\rho)\cot t\, dt, \qquad 0 < \rho < \pi/4.$$

On this interval it is finite, has $J'(\rho) < 0$, and tends to infinity as $\rho \downarrow 0$. For a sufficiently small regularization parameter $d > 0$, set

$$\ell_e = -\log \beta_e, \qquad \delta_e = \frac{d\ell_e}{1+\ell_e}, \qquad J(\rho) = \frac{1+\ell_e}{d}.$$

The last equation has a unique solution $0 < \rho < \pi/4$, smooth in the parameters by $J'(\rho) \neq 0$. Although $\delta_e = 0$ at $\beta_e = 1$, the equation defining $\rho$ remains regular there. Now put

$$z(t) = -\delta_e \chi(t/\rho), \qquad y(t) = \exp\left(\int_0^t z(v)\cot v\, dv\right), \qquad b_{\beta_e,d}(t) = \sin t\, y(t). \tag{5.2}$$

Near 0 the integrand vanishes, so $b_{\beta_e,d} = \sin t$ exactly. For $t \geq \rho$,

$$\int_0^t \chi(v/\rho)\cot v\, dv = J(\rho) + \log\sin t, \qquad \delta_e J(\rho) = \ell_e,$$

and hence

$$b_{\beta_e,d}(t) = \beta_e(\sin t)^{1-\delta_e}. \tag{5.3}$$

This profile replaces $\beta_e \sin t$ in the raw tensor.

At the first endpoint the metric is exactly the round join metric near the collapsing circle, multiplied by $A^2$. At the other endpoint use $v = \pi/2 - t$; the tensor divided by $A^2$ becomes

$$dv^2 + \sin^2 v\, g_{S^{m-2}} + \beta_e^2(\cos v)^{2(1-\delta_e)} d\theta^2.$$

The normal polar part is smooth, and the last coefficient is a smooth even function of $v$. Thus both collapsed strata are smooth. If $\beta_e = 1$, then $\delta_e = 0$ and the entire metric is $A^2 g_{S^m}$.

The curvature operator of the unscaled doubly warped tensor is diagonal on radial–sphere, sphere–sphere, sphere–circle and radial–circle two-vectors. Its eigenvalues are, respectively,

$$1, \qquad 1, \qquad 1+z, \qquad -\frac{b''}{b} = 1 + z - z'\cot t - z(1+z)\cot^2 t. \tag{5.4}$$

The sphere–sphere summand is absent for $m = 3$. Since $-d < z \leq 0$, $z' \leq 0$ and $1 + z > 0$, all eigenvalues are at least $1 - d$. A unit simple two-vector is a unit vector in this orthonormal eigenbasis, so its sectional curvature is a weighted average of these eigenvalues. Restoring $A^2$ gives

$$\sec_{\mathcal{G}(A,\beta_e,d)} \geq A^{-2}(1-d).$$

Thus the curvature bound covers arbitrary two-planes, not only the four coordinate types. [N, Lemma 5.2, equations (5.10)–(5.11)].

Two further estimates explain the volume and metric limits. Monotonicity gives $\beta_e \leq y \leq 1$ and $\rho \leq \pi e^{-1/d}$. The volume surplus is

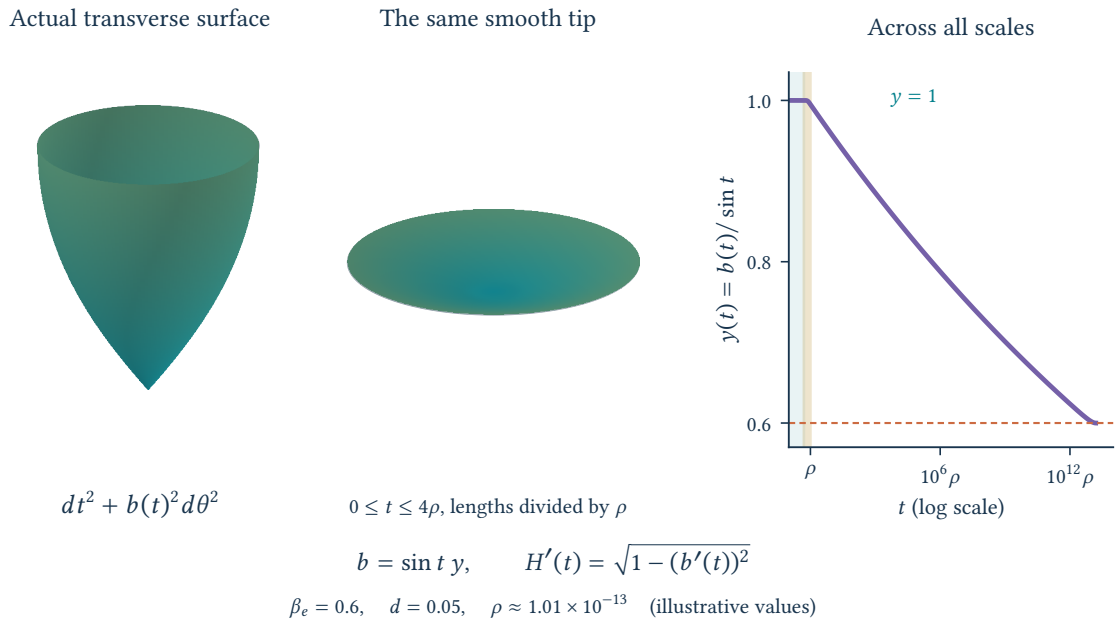
$$\frac{\mathrm{Vol}(\mathcal{G}) - \mathrm{Vol}(g^{\mathrm{raw}})}{A^m} = 2\pi\sigma_{m-2}\int_0^{\pi/2} \cos^{m-2} t \sin t\,(y - \beta_e)\, dt \geq 0.$$

The interval $[0,\rho]$ contributes $O(\rho^2)$. On $[\rho,\pi/2]$, the bound

$$0 \leq x^{-\delta_e} - 1 \leq \delta_e |\log x| x^{-1/2}, \qquad 0 < x \leq 1,$$

follows from the mean-value theorem when $\delta_e < 1/2$. The resulting integrand is bounded by a constant times $d\cos^{m-2} t \sin^{1/2} t|\log\sin t|$, which is integrable. After the preliminary smallness choice, $\rho^2 \le d$, and

$$0 \le \mathrm{Vol}(\mathcal{G}) - \mathrm{Vol}(g^{\mathrm{raw}}) \le C_m A^m d. \tag{5.5}$$




VISUAL B. The actual transverse metric $dt^2 + b(t)^2 d\theta^2$ represented as a surface of revolution, with radius $b(t)$ and height derivative $\sqrt{1-(b'(t))^2}$. The middle panel shows the same surface for $0 \le t \le 4\rho$, with every length divided by $\rho$; its centre is a smooth round germ. The logarithmic plot resolves the ratio $y = b/\sin t$ across the intervening scales. These are two-dimensional transverse slices, not embeddings of the full higher-dimensional metric. The illustrative values do not assert the thresholds of the full construction.

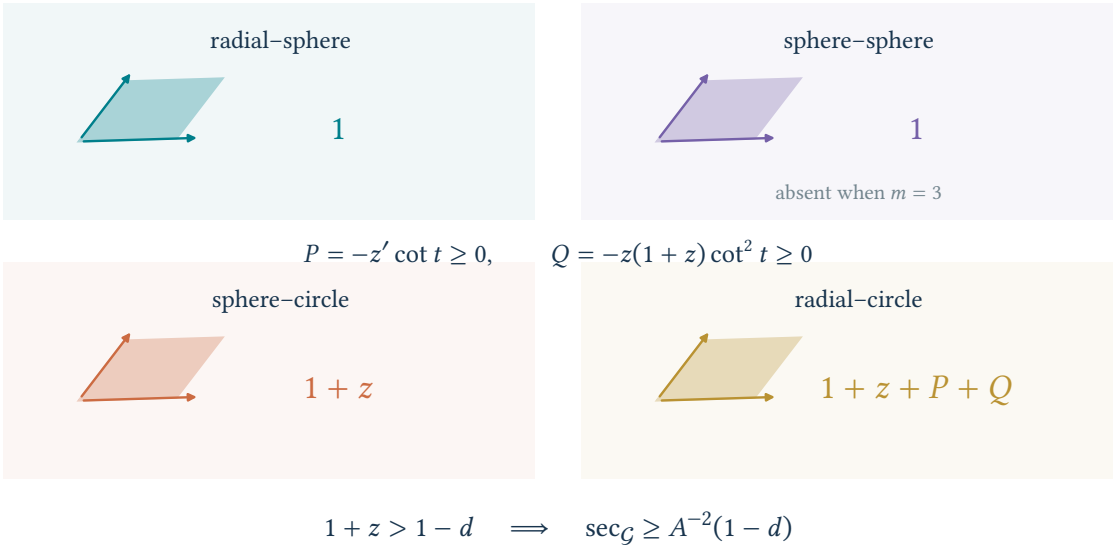
Let $d_0, d_1$ denote the raw and smoothed length distances on the common quotient. The coefficient inequality gives $d_0 \le d_1$. For $\rho \le \eta < 1/4$, the outer region $t \ge \eta$ has length ratio at most $\exp(d|\log\sin\eta|)$. For a nearly minimizing raw curve that enters $t \le \eta$, consider its entire first-to-last passage through that region. Keep its radial and sphere coordinates but make the angular coordinate constant on this passage. Restore the two endpoint angles by shortest circle arcs, each of length at most $\pi A\eta$. The central path now has equal length in both metrics and no greater length than before. Consequently

$$d_0 \le d_1 \le e^{d|\log\sin\eta|} d_0 + 2\pi A\eta. \tag{5.6}$$

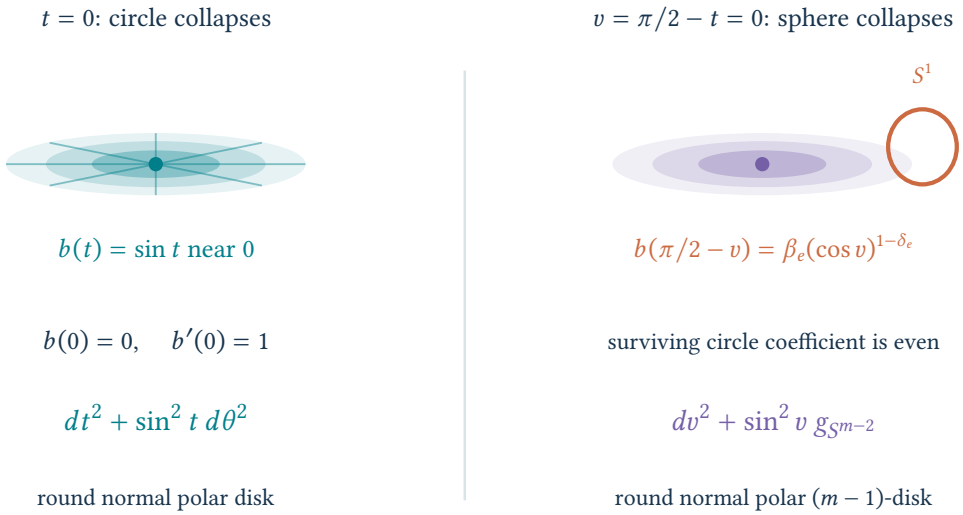
Curves in endpoint strata are obtained as limits of parallel regular-stratum curves, so the same inequality applies to the completed distances. Since $\operatorname{diam} d_0 \le 2\pi A$, taking $\eta = \sqrt{d}$ bounds the distortion of the identity correspondence by

$$C_m A\big(\sqrt{d} + d|\log\sin\sqrt{d}|\big) \longrightarrow 0.$$

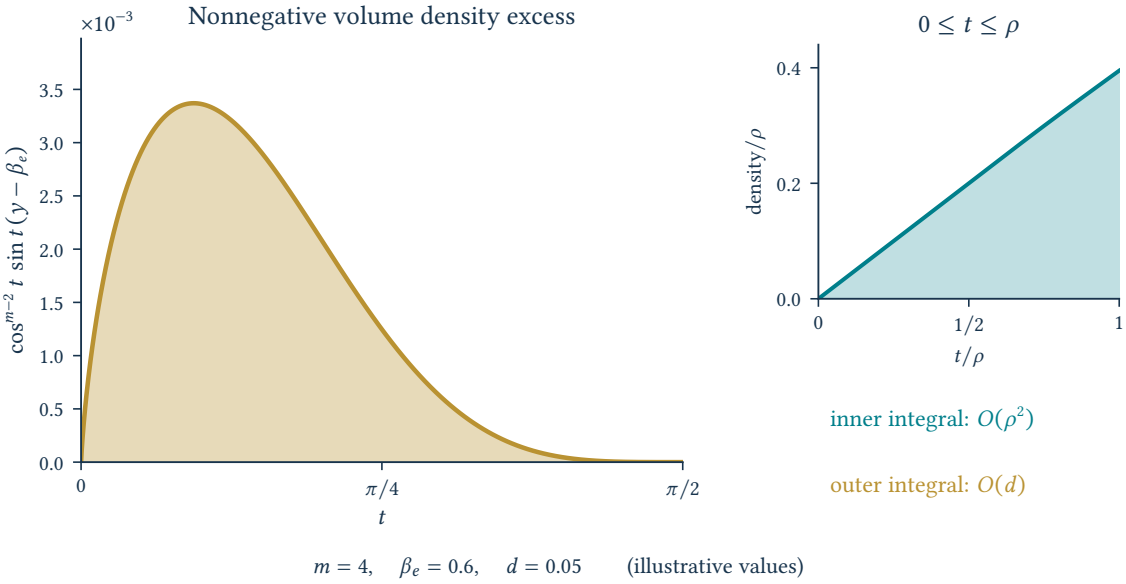
A thin edge tube need not have small diameter along the edge; it is the small cost of changing its *angular* coordinate that proves this estimate. [N, Lemma 5.2, equations (5.15)–(5.18)]. In Visual F, follow the constant angular track across the intervening radial excursion; the radial and sphere coordinates are retained.



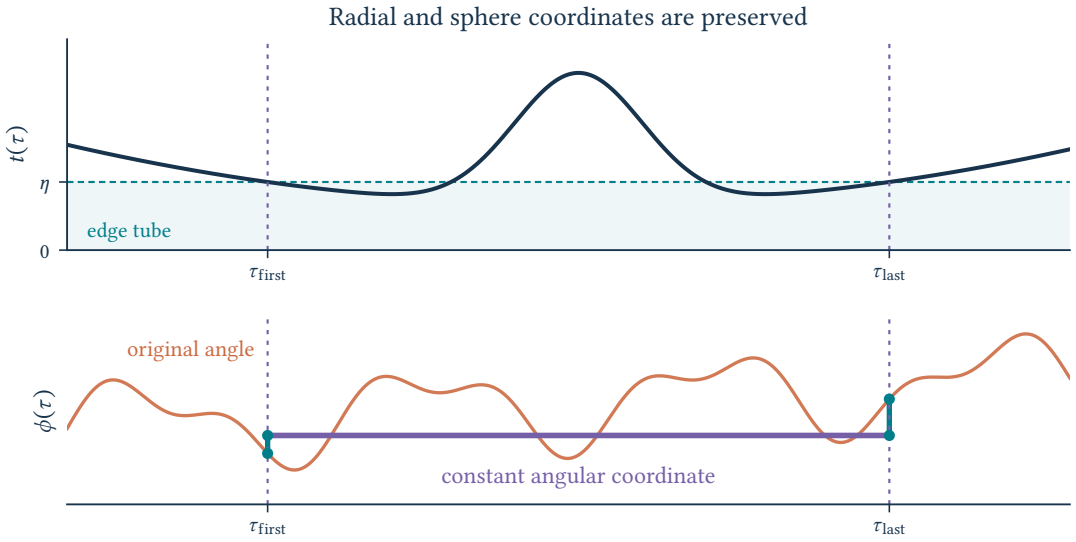

VISUAL C. The four orthogonal curvature-operator blocks of the unscaled doubly warped tensor. In the radial–circle block, both additional contributions $P$ and $Q$ are nonnegative. Every unit simple two-vector has curvature equal to a weighted average of these eigenvalues; scaling the metric by $A^2$ multiplies sectional curvature by $A^{-2}$. The plane symbols identify coordinate types and do not encode their multiplicities.




VISUAL D. The two smooth endpoint germs, with the common factor $A^2$ suppressed. At the first endpoint the collapsing circle has the exact round polar profile. At the second, the collapsing sphere has a round polar normal tensor and the surviving circle has a smooth even coefficient in $v$. The fibre symbols are coordinate schematics; they do not depict an embedding of the complete higher-dimensional sphere.




VISUAL E. The excess volume is the shaded integral, multiplied by $2\pi\sigma_{m-2}A^m$. The right panel magnifies the actual interval $[0, \rho]$, with its density divided by $\rho$ and its coordinate divided by $\rho$; returning to the original variables supplies the factor $\rho^2$. The remaining interval is controlled by the integrable logarithmic bound in the text. Both plots use the same actual profile as the preceding profile illustration.




Each endpoint arc costs at most $\pi A\eta$; the middle path has no angular cost.

VISUAL F. The entire first-to-last passage is replaced, including any intervening excursion outside the tube. The upper track records the unchanged radial coordinate; the sphere coordinate is also retained. The lower track records an illustrative continuous angular lift: set this angle constant on the full middle interval and attach shortest circle arcs at its two endpoints. Their total cost is at most $2\pi A\eta$. The drawn curves illustrate the replacement, not a computed minimizing geodesic.

**The two-parameter path and its exact volume.** Let $\vartheta(s)$ be zero on an initial interval, increase smoothly to one without reaching it, and set

$$\gamma(s) = q + (\gamma_* - q)(1 - \vartheta(s)), \qquad a(s) = \big(\gamma_* + (1 - \gamma_*)\vartheta(s)\big)^{1/m}.$$

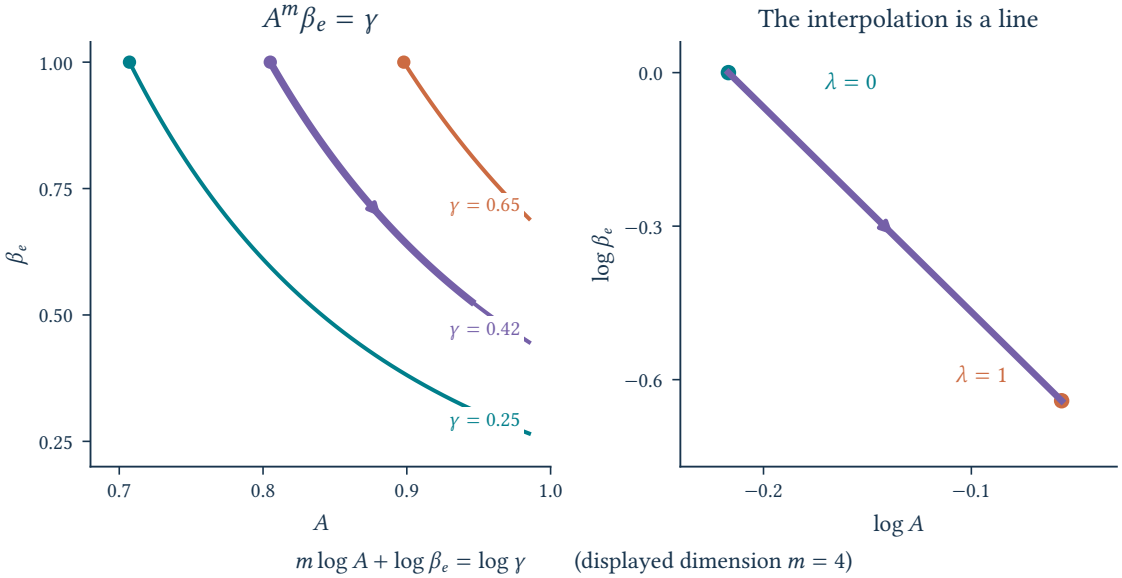
The manuscript takes $\vartheta(s) = e^{-1/(s-1)}$ for $s > 1$ and zero for $s \le 1$; a reparametrization enlarges the initial constant interval when required later. We have $a^m - \gamma = (1 - q)\vartheta \ge 0$. If $\lambda(u)$ is a smooth step from zero to one, constant near $u = -2$ and $u = 2$, the logarithmic interpolation of [N, Theorem 5.3] can be written

$$A(s,u) = \gamma(s)^{(1-\lambda(u))/m} a(s)^{\lambda(u)}, \qquad \beta_e(s,u) = \left(\frac{\gamma(s)}{a(s)^m}\right)^{\lambda(u)}. \tag{5.7}$$

Indeed, these are the first equal coordinates and the ratio of the last to the first coordinate in the interpolated suspension parameters. Thus

$$A(s,u)^m \beta_e(s,u) = \gamma(s), \qquad q < \gamma(s) \le \beta_e(s,u) \le 1, \qquad 0 < A(s,u) < 1.$$

The product identity is what fixes the raw volume throughout the $u$-path.




VISUAL G. The raw-volume constraint is a level curve in the $(A, \beta_e)$ plane and a straight line in logarithmic coordinates. The highlighted path follows (5.7) from $(\gamma^{1/m}, 1)$ to $(a, \gamma/a^m)$. The displayed values $m = 4$, $\gamma = 0.42$, $a = 0.945$ illustrate this identity; they do not represent a choice of the final construction constants.

Choose, exactly as in the manuscript,

$$d(s,u) = \frac{d_*}{8}\frac{1 - A(s,u)^2}{2 - A(s,u)^2}(1 - \vartheta(s))^4, \qquad 0 < d_* < 1/16.$$

For every finite $s$, this is positive and smaller than both $d_*$ and $1 - A^2$. Hence $\widetilde{g}_{s,u} = \mathcal{G}(A, \beta_e, d)$ has sectional curvature greater than one and Ricci curvature at least $(m-1)\widetilde{g}_{s,u}$. By (5.5), its volume is at least $\gamma(s)\sigma_m$. Put

$$\xi(s,u)^m = \frac{\gamma(s)\sigma_m}{\mathrm{Vol}(\widetilde{g}_{s,u})}, \qquad \widehat{g}_{s,u} = \xi(s,u)^2 \widetilde{g}_{s,u}.$$

Then $0 < \xi \le 1$, so this homothety fixes the total volume without weakening the required normalized Ricci inequality:

$$\mathrm{Vol}(\widehat{g}_{s,u}) = \gamma(s)\sigma_m, \qquad \mathrm{Ric}_{\widehat{g}_{s,u}} \ge (m-1)\widehat{g}_{s,u}.$$

At $u = -2$ the metric is exactly $\gamma(s)^{2/m} g_{S^m}$. At $u = 2$, the parameters satisfy $A \to 1$, $\beta_e \to q$, $d \to 0$, and (5.5) implies $\xi \to 1$. The distance estimate (5.6), followed by coefficient comparison of the raw joins, proves $h_s := \widehat{g}_{s,2} \to B_{n,q}$. At the initial constant interval the whole $u$-path is round. Smooth parameter dependence and endpoint constancy are preserved at every step. [N, Theorem 5.3].

**A surface model for the opening angle.** Figure 6 is an optional surface model; Visual B displays the actual transverse profile. For this model, set

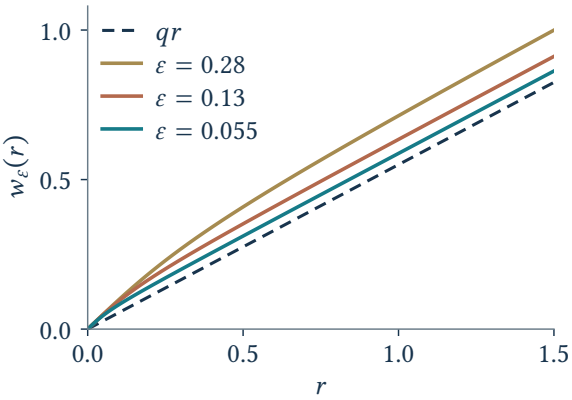
$$w_\varepsilon(r) = qr + (1-q)\varepsilon \arctan(r/\varepsilon).$$

Then $w_\varepsilon' = q + (1-q)/(1+(r/\varepsilon)^2)$ and $w_\varepsilon'' = -2(1-q)r/[\varepsilon^2(1+(r/\varepsilon)^2)^2]$. Thus $dr^2 + w_\varepsilon^2 d\phi^2$ has nonnegative Gaussian curvature and a smooth pole, since

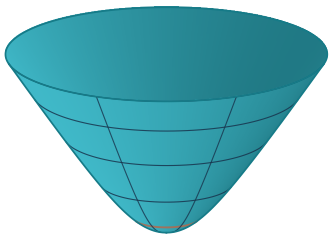
$$w_\varepsilon(r) = r - \frac{1-q}{3\varepsilon^2} r^3 + O(r^5), \qquad K(0) = \frac{2(1-q)}{\varepsilon^2}.$$

Also $0 \le w_\varepsilon - qr \le (1-q)\pi\varepsilon/2$. Its surface of revolution has height derivative $\sqrt{1-(w_\varepsilon')^2}$. This model explains the change from smooth initial slope to a shorter-circle cone. It is not the higher-dimensional profile (5.2).

(a) Radius profiles




(b) Surface, $\varepsilon = 0.13$



smooth pole

FIGURE 6. The illustrative smooth surfaces with $w_\varepsilon = qr + (1-q)\varepsilon \arctan(r/\varepsilon)$ and $q = 0.55$. The surface uses $\varepsilon = 0.13$. Its Gaussian curvature is nonnegative. The actual sphere regularization is (5.2), with the curvature and distance estimates proved above.

## 6. A SUSPENSION WITH TWO TOPOLOGICAL CAPS

*The manifold is fixed; only the sizes of its distinguished regions change.*

The suspension over $h_s$ has tensor $dt^2 + \sin^2 t\, h_s$ on $0 < t < \pi$. Its radial Ricci curvature is $n-1$. For an $h_s$-unit vector $v$, its value on $(\sin t)^{-1} v$ is

$$\frac{\mathrm{Ric}_{h_s}(v,v) + \sin^2 t - (n-2)\cos^2 t}{\sin^2 t} \ge n-1;$$

the mixed component vanishes. Cut at $t = \varepsilon$ and $t = \pi - \varepsilon$. Oppositely oriented copies of $P_Q$, attached by the fixed compatible boundary maps, produce

$$P_Q \cup_{S^{n-1}} ([0,1] \times S^{n-1}) \cup_{S^{n-1}} (-P_Q) \cong Q\#(-Q).$$

No change of underlying smooth manifold occurs as $s$ varies. [N, §4.2 and §8].

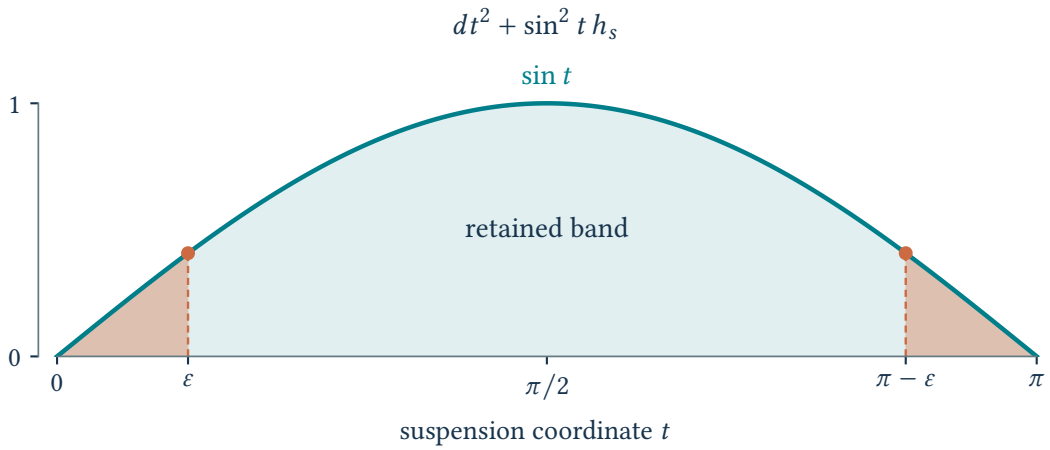



FIGURE 7. The exact suspension warping graph $\sin t$, cut at $\varepsilon$ and $\pi - \varepsilon$. Both boundary tensors are $\sin^2 \varepsilon\, h_s$. The polar intervals locate the replacements; their planar areas are not volumes.

**The cap output.** For the fixed input family there are $\varepsilon_0, C, D, V > 0$ and a smooth family of metrics $K_{s,\varepsilon}$ on the fixed $P_Q$, for all $s \geq 0$ and $0 < \varepsilon < \varepsilon_0$, such that

$$\begin{aligned} \beta_Q^*(K_{s,\varepsilon}|_{\partial P_Q}) &= \sin^2 \varepsilon\, h_s, \\ \beta_Q^* \mathrm{II}_{\partial P_Q, K_{s,\varepsilon}} &> \cot \varepsilon\, \sin^2 \varepsilon\, h_s, \\ \mathrm{Ric}_{K_{s,\varepsilon}} &\geq (n - 1 - C\varepsilon^2) K_{s,\varepsilon}, \\ \mathrm{diam}(P_Q, K_{s,\varepsilon}) \leq D\varepsilon, \qquad & \mathrm{Vol}(P_Q, K_{s,\varepsilon}) \leq V\varepsilon^n. \end{aligned}$$

Diameter here uses the intrinsic length distance of the whole cap. The constants are independent of $s$; this does not assert uniform bounds for every $s$-derivative of the family. Relative choices retain an initial reference cap exactly, and synchronized choices respect the map exchanging the two copies. [N, Proposition 7.6].

Sections 8–9 explain why these properties can hold simultaneously. The final choice $\varepsilon = \varepsilon(s)$ also has to satisfy the volume-error conditions in Section 10.

After the outer seam is smoothed, enlarge each cap by its smoothing collar and the remaining suspension strip up to $2\varepsilon$; call these polar domains $E_s^{\pm}$. The protected exterior is exactly the corresponding suspension band. Radial paths to the slice $t = 2\varepsilon$, intrinsic collar paths, and the cap diameter bound give

$$\mathrm{diam}^{\mathrm{int}}\, E_s^{\pm} \leq (2D + 8 + 6\pi)\varepsilon.$$

The deleted polar domains $P_s^{\pm}$ in the complete suspension satisfy $\mathrm{diam}^{\mathrm{int}}\, P_s^{\pm} \leq (4 + 2\pi)\varepsilon$. To compare two exterior points, replace the entire first-to-last passage through the minus domain, then do the same for the plus domain. The second replacement may erase part of the first path, but adds at most its own intrinsic diameter. Reverse the procedure for the opposite inequality. This controls *ambient* distances in both spaces, even when an exterior shortcut enters a cap.

Relate identical exterior points, all points of each $E_s^{\pm}$ to the corresponding suspension pole, and one chosen point of $E_s^{\pm}$ to every point of $P_s^{\pm}$. This is surjective in both factors. With $\Delta_s^{\pm} = \mathrm{diam}^{\mathrm{int}}\, E_s^{\pm} + \mathrm{diam}^{\mathrm{int}}\, P_s^{\pm}$, boundary anchors and the preceding path replacements give distortion at most $2\Delta_s^- + 2\Delta_s^+$. Thus the raw capped links approach the suspension of $h_s$ as $\varepsilon(s) \to 0$. Suspension preserves the convergence $h_s \to B_{n,q}$ by its distance formula and uniform continuity of arccos on $[-1, 1]$. Hence

$$(M_Q, \widehat{G}_s) \longrightarrow L_{n,q}.$$

This argument uses intrinsic sizes of replacement domains, not a false equality of ambient distances on the common exterior. [N, Theorem 8.1, equations (8.11), (8.15)–(8.17)].

## 7. What shrinks, and what remains

*The five-dimensional example makes the two limits tangible.*

For $Q = \mathbb{CP}^2$, every finite link is $M = \mathbb{CP}^2\#(-\mathbb{CP}^2)$. Its two punctured cores carry classes $\alpha_+, \alpha_-$ generating $H_2(M;\mathbb{Z}) = \mathbb{Z}^2$. Their containing cap regions have diameter tending to zero, but their classes exist at every finite stage. The limiting link is homeomorphic to $S^4$, whose second homology vanishes.

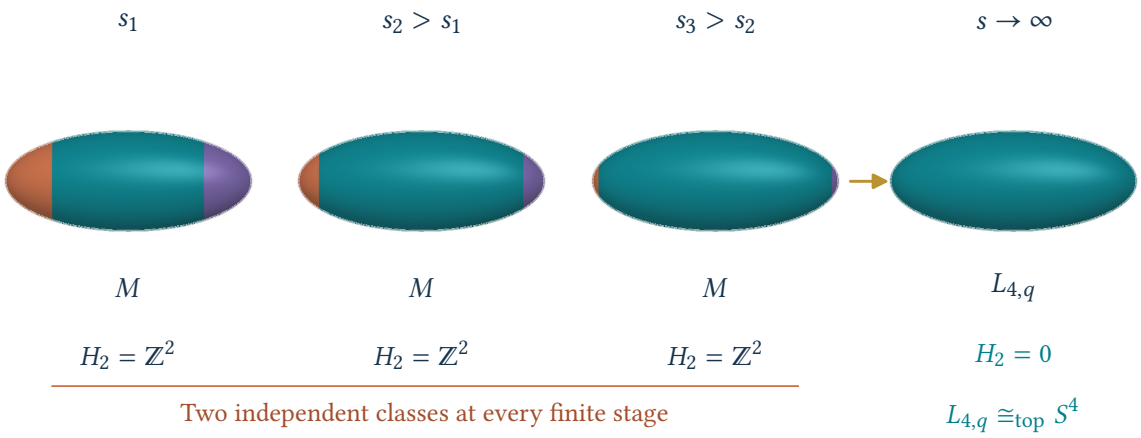



Figure 8. The cap regions shrink, but every finite link remains $\mathbb{CP}^2\#(-\mathbb{CP}^2)$, with $H_2 = \mathbb{Z}^2$. The limit link is homeomorphic to $S^4$. The shaded bodies indicate regions in four-dimensional links, not embeddings of those links in three-space.

A punctured neighbourhood in the radial completion still retracts onto the fixed $M$. A tangent instead uses the metric limit of the changing metrics on $M$. No continuity of singular homology under Gromov–Hausdorff convergence is asserted or needed. [N, §4 and §10].

## 8. Why the seams can be smoothed

*Boundary metric matching is only the first requirement.*

For a collar $du^2 + k(u)$ whose inward normal is $\partial_u$, our second fundamental form is $-k'(0)/2$. At either end of the retained suspension band it is $-\cot\varepsilon\, g_\partial$. The required cap inequality therefore gives

$$\mathrm{II}_{\text{cap}} + \mathrm{II}_{\text{band}} > 0.$$

We must construct the cap with this inequality, not assume that a scaled core has it. There are two separate internal seams and a third, outer attachment to the suspension.

**The volume form inside the cap.** Fix $s$. The path $\widehat{g}_{s,u}$ on $S^{n-1}$ from Section 5 has constant *total* volume in $u$. Put $\omega_{s,u} = dv_{\widehat{g}_{s,u}}$ and $\alpha_{s,u} = \partial_u \omega_{s,u}$. Since $\int \alpha_{s,u} = 0$, Hodge theory for one fixed background metric gives

$$\eta_{s,u} = d^*\mathcal{G}\alpha_{s,u}, \qquad d\eta_{s,u} = \alpha_{s,u}.$$

Here $\mathcal{G}$ is the Green operator on top-degree forms. Define $X_{s,u}$ by $\iota_{X_{s,u}}\omega_{s,u} = -\eta_{s,u}$ and let $\phi_{s,u}$ be its flow, starting at the identity for $u = -2$. Compactness of the sphere gives existence over the whole finite $u$-interval and smooth dependence on $s$. Cartan's formula gives

$$\partial_u(\phi_{s,u}^*\omega_{s,u}) = \phi_{s,u}^*(\alpha_{s,u} + d\iota_{X_{s,u}}\omega_{s,u}) = 0.$$

Thus $g_{s,u} = \phi_{s,u}^* \widehat{g}_{s,u}$ has a common volume form in $u$ and retains the Ricci bound. Stationary endpoints make the vector field zero there. Crucially,

$$g_{s,-2} = \tau_s^2 g_{S^{n-1}}, \qquad g_{s,2} = \phi_{s,2}^* h_s.$$

The fixed volume form may depend on $s$. This is not yet the later normalization on the closed manifold $M_Q$. [N, Theorem 5.3; Theorem 7.5; Proposition 7.6].

**From spherical tuning to a boundary surplus.** The slowed path is placed in a radial transition with factor

$$a_\varepsilon(r) = \frac{\sin(\kappa_\varepsilon r)}{\kappa_\varepsilon} \chi_\varepsilon(r),$$

where the endpoint estimates give $1 - \varepsilon^4 \le \chi_\varepsilon(1) \le 1$ and $|\chi_\varepsilon'(1)| \le \varepsilon^4$. The exact tuning is

$$\lambda_\varepsilon = \sqrt{\sin^2 \varepsilon - 8\varepsilon^4}, \qquad \chi_\varepsilon(1) \sin \kappa_\varepsilon = \lambda_\varepsilon, \qquad \varepsilon/2 \le \kappa_\varepsilon \le 4\varepsilon < 1/2.$$

All these statements are for sufficiently small positive $\varepsilon$; the threshold is fixed in the spherical-deformation construction. Put

$$c_\varepsilon = \frac{\sin \varepsilon \, \kappa_\varepsilon}{\lambda_\varepsilon}, \qquad c_\varepsilon a_\varepsilon(1) = \sin \varepsilon.$$

The derivative surplus follows rather than being an additional assumption. Indeed,

$$\chi_\varepsilon(1)^2 - \lambda_\varepsilon^2 - \cos^2 \varepsilon = \chi_\varepsilon(1)^2 - 1 + 8\varepsilon^4 \ge 6\varepsilon^4.$$

Both terms in the denominator of the rationalized square-root difference are positive and at most one, so

$$\sqrt{\chi_\varepsilon(1)^2 - \lambda_\varepsilon^2} - \cos \varepsilon \ge 3\varepsilon^4.$$

It follows that

$$a_\varepsilon'(1) = \sqrt{\chi_\varepsilon(1)^2 - \lambda_\varepsilon^2} + \frac{\sin \kappa_\varepsilon}{\kappa_\varepsilon} \chi_\varepsilon'(1) \ge \cos \varepsilon + 2\varepsilon^4. \tag{8.1}$$

The link path is stationary near $r = 1$. With inward normal $-\partial_r$, and then scaling the whole transition by $c_\varepsilon^2$, its outer form is

$$\mathrm{II}_\partial = \frac{a_\varepsilon'(1)}{\sin \varepsilon} g_\partial \ge \left( \cot \varepsilon + \frac{2\varepsilon^4}{\sin \varepsilon} \right) g_\partial. \tag{8.2}$$

This is the source of the strict gluing margin. [N, Theorem 6.1, equations (6.49)–(6.51); Proposition 7.6, equations (7.90)–(7.94)].

The spherical replacement also requires a full Ricci estimate. Compare $a_\varepsilon$ with $b = r\chi_\varepsilon$ and put $d_\kappa = \kappa \cot(\kappa r) - 1/r$. Then

$$d_\kappa = -\kappa^2 r/3 + O(\kappa^4 r^3).$$

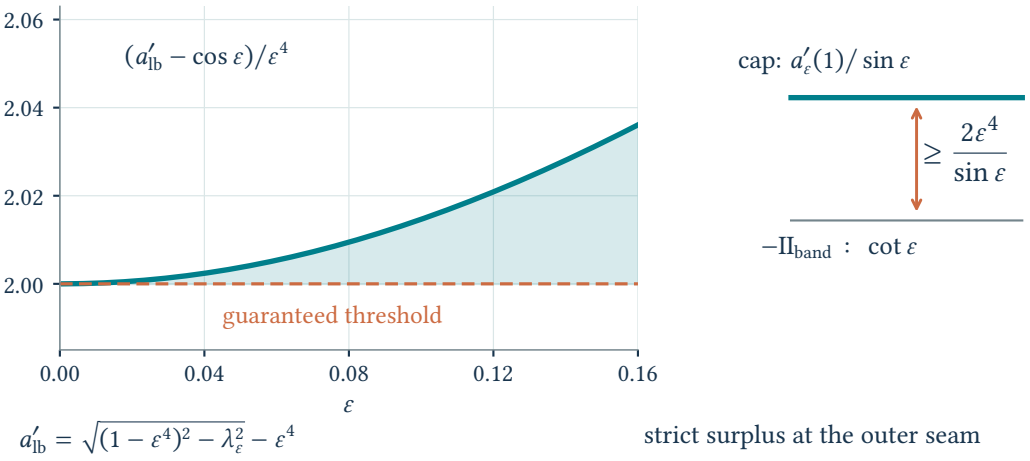
The radial Ricci difference equals $(n-1)\kappa^2 + O(\varepsilon^4 \kappa^2)$. In the respective unit frames $a_\varepsilon^{-1} e$ and $b^{-1} e$, the tangential difference is bounded *below* by $(n-1)\kappa^2 - C(\varepsilon^4 \kappa^2 + \kappa^4)$. This is a one-sided estimate: the coefficient $a_\varepsilon^{-2} - b^{-2}$ is nonnegative, so the link bound $\mathrm{Ric}_g \ge (n-2)g$ gives its lower contribution. The three leading lower coefficients sum to $(n-2)/3 + 1 + 2(n-2)/3 = n - 1$; no uniform upper bound on link Ricci is assumed. The mixed difference is

$$\left( \frac{b}{a_\varepsilon} - 1 \right) \mathrm{Ric}_{G_0}(\partial_r, b^{-1} e) = O(\varepsilon^4 \kappa^2),$$

using $b/a_\varepsilon = \kappa r / \sin(\kappa r)$ and the weighted mixed estimate for $G_0$. Testing an arbitrary unit vector and using $2|xy| \le x^2 + y^2$ yields the tensor bound in [N, Theorem 6.1]. Finally,

$$\frac{\kappa_\varepsilon^2}{c_\varepsilon^2} = \frac{\lambda_\varepsilon^2}{\sin^2 \varepsilon} = 1 - \frac{8\varepsilon^4}{\sin^2 \varepsilon} = 1 - O(\varepsilon^2)$$

converts it to $\mathrm{Ric} \ge (n - 1 - C\varepsilon^2)g$ after scaling. The quoted error bounds are the component estimates of [N, equations (6.43)–(6.48)], including the mixed block.




VISUAL H. A quantitative lower bound for the outer slope surplus. The curve uses $a'_{\mathrm{lb}} = \sqrt{(1-\varepsilon^4)^2 - \lambda_\varepsilon^2} - \varepsilon^4 \leq a'_\varepsilon(1)$, obtained from the endpoint bounds and $\sin\kappa_\varepsilon/\kappa_\varepsilon \leq 1$. Rationalization gives $(a'_{\mathrm{lb}} - \cos\varepsilon)/\varepsilon^4 \geq 2$. The right diagram records the resulting coefficient gap in the gluing comparison, with schematic spacing. The displayed interval illustrates the algebraic lower envelope; the geometric construction uses sufficiently small $\varepsilon$ satisfying all preceding restrictions.

**The two internal seams.** At a sufficiently small inner slice the link is round. Before the final homothety let $b, c$ be its radius and outward radial derivative, and write

$$d_c = \bar{\kappa}_Q/2, \qquad e_c = 3\bar{\kappa}_Q/4, \qquad s_c = b\sqrt{\frac{1-e_c^2}{1-d_c^2}}.$$

The subscripts distinguish these constants from the edge regularization parameter $d$. The construction ensures $c \leq \tau_s < \bar{\kappa}_Q/4 < d_c < e_c < \kappa_Q$. A round annulus with curvature scale $\Lambda = \sqrt{1-d_c^2}/b$ has radius and derivative $(b, d_c)$ at $T_d = \arccos(d_c)/\Lambda$ and $(s_c, e_c)$ at $T_e = \arccos(e_c)/\Lambda$. Therefore the two internal sums are

$$\mathrm{II}_{\mathrm{transition}} + \mathrm{II}_{\mathrm{round}} = \frac{d_c - c}{b}\, b^2 g_{S^{n-1}} > 0,$$
$$\mathrm{II}_{\mathrm{annulus}} + \mathrm{II}_{\mathrm{core}} \geq \frac{\kappa_Q - e_c}{s_c}\, s_c^2 g_{S^{n-1}} > 0.$$

The scaled core is $(P_Q, s_c^2 k_Q)$. Both equalities of boundary metrics use the fixed sphere coordinates. [N, equations (7.96)–(7.99)].

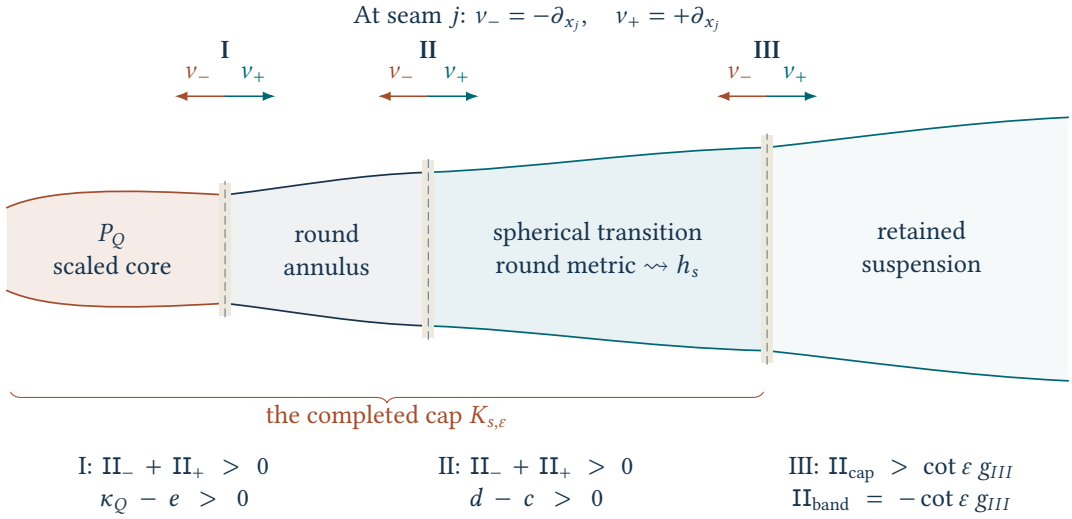
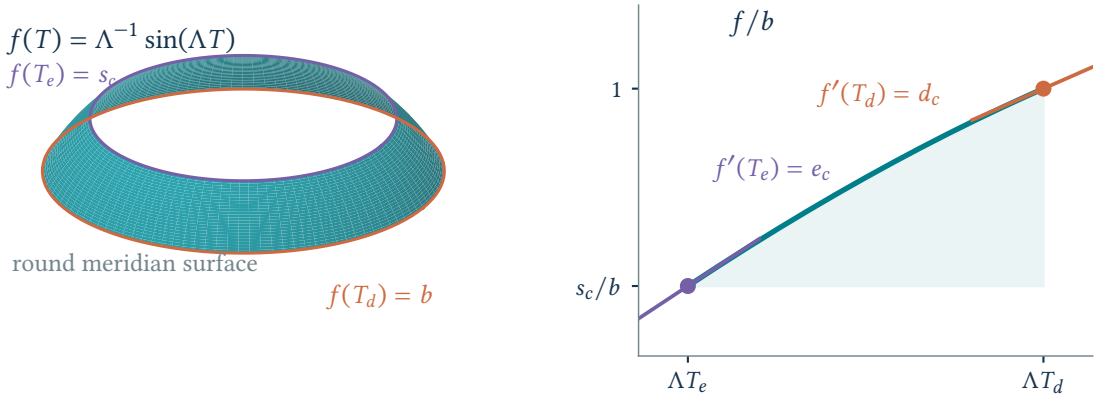



FIGURE 9. The three interfaces. In this retained illustration the constants $d, e$ mean $d_c, e_c$ of the text. Signed unit coordinates increase to the right, with the two inward normals pointing into their respective pieces. The internal margins are $(\kappa_Q - e_c)/s_c$ and $(d_c - c)/b$; the outer cap surplus is (8.2).




$$s_c/b = \sqrt{(1-e_c^2)/(1-d_c^2)} \qquad e_c = 3/4, \quad d_c = 1/2$$

VISUAL I. The round annulus has radius function $f(T) = \Lambda^{-1}\sin(\Lambda T)$. Its two boundary radii and slopes lie on one exact profile. The surface shows a two-dimensional round meridian; the full annulus has fibre $S^{n-1}$. The illustrative normalization $\bar{\kappa}_Q = b = 1$ preserves the displayed dimensionless ratio $s_c/b$; no embedding of the full annulus is asserted.

The inner slice is also chosen to make both inserted round and core Ricci coefficients exceed the transition coefficient $\mathcal{R}_\varepsilon > 0$:

$$\frac{(n-1)(1-d_c^2)}{b^2} > \mathcal{R}_\varepsilon, \qquad \frac{\mu_Q(1-d_c^2)}{(1-e_c^2)b^2} > \mathcal{R}_\varepsilon.$$

There is a smooth way to make this choice, rather than selecting an unrelated radius for each $s$. With $r_-(s,\varepsilon)$ the end of the round interval, set

$$Q_1 = \frac{(n-1)(1-d_c^2)}{\tau_s^2 \mathcal{R}_\varepsilon}, \quad Q_2 = \frac{\mu_Q(1-d_c^2)}{(1-e_c^2)\tau_s^2 \mathcal{R}_\varepsilon}, \quad r_c = \frac{1}{4}(1 + r_-^{-2} + Q_1^{-1} + Q_2^{-1})^{-1/2}.$$

Then $r_c < r_-/4$ and $r_c^2 < Q_i/16$. Since $b \le \tau_s r_c$, the required strict Ricci inequalities follow. The first smoothing is confined near $T_d$ and preserves a neighbourhood of $T_e$; the second is confined near $T_e$. Their supports are disjoint, and both leave the outer transition boundary unchanged. [N, Proposition 7.6].

**Restore the prescribed boundary tensor.** Before its final collar pullback, the cap boundary is $\sin^2 \varepsilon\, \phi_{s,2}^* h_s$. An isometric boundary with an unspecified parametrization is not yet the displayed cap output. On a fixed collar $[0,1] \times \partial P_Q$ choose $\vartheta_0 = 1$ near zero and $\vartheta_0 = 0$ for $t \ge 1/2$. Put $\widehat{\phi}_{s,u} = \beta_Q \phi_{s,u} \beta_Q^{-1}$ and define

$$\mathcal{F}_s(t,x) = \big(t, \widehat{\phi}^{-1}_{s,-2+4\vartheta_0(t)}(x)\big),$$

extending by the identity off the collar. The inverse uses $\widehat{\phi}$ in place of $\widehat{\phi}^{-1}$, so this is a smooth family of diffeomorphisms. On the boundary, $\mathcal{F}_s \beta_Q = \beta_Q \phi_{s,2}^{-1}$. Pulling the cap metric back by $\mathcal{F}_s$ therefore gives

$$(\phi_{s,2}^{-1})^*(\sin^2 \varepsilon\, \phi_{s,2}^* h_s) = \sin^2 \varepsilon\, h_s$$

under the fixed map $\beta_Q$. Ricci, intrinsic sizes and the second fundamental form inequality are preserved by this isometry. This is the exact identification required at the outer suspension seam. [N, Proposition 7.6, p. 65].

## 9. Why parameters and symmetry are part of the theorem

*A pointwise cap is not yet a usable family of metrics.*

The parameters have distinct roles: $s$ moves towards the singular sphere link, $u$ interpolates inside one cap, and $r$ is the cap's radial coordinate. Smoothness on compact $s$-intervals does not give uniform bounds as $s \to \infty$. Let $B(s)$ bound the sum of the supremum norms of $\partial_u g$, $\partial_u^2 g$ and $\nabla \partial_u g$ on the stationary-extended $u$-path. It is finite and continuous. Choose a smooth majorant $A_{\mathrm{maj}}(s) > B(s)$, a stationary smooth step $\rho_0$ from $-2$ to 2, and set

$$L(s) = c_\rho(1 + A_{\mathrm{maj}}(s))^2, \qquad k_{s,v} = g_{s,\rho_0(v/L(s))}.$$

If $a_1 = \|\rho_0'\|_\infty$, $a_2 = \|\rho_0''\|_\infty$ and $c_\rho \ge \max\{1, 4a_1, \sqrt{2(a_2 + a_1^2)}\}$, the chain rule gives

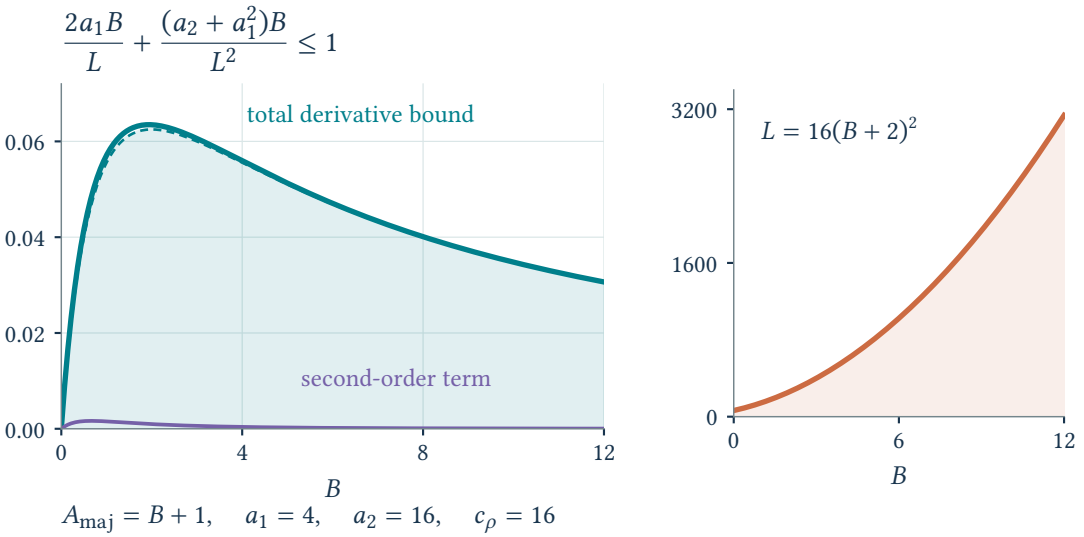
$$\|\partial_v k\| + \|\partial_v^2 k\| + \|\nabla \partial_v k\| \le \frac{2a_1 B(s)}{L(s)} + \frac{(a_2 + a_1^2)B(s)}{L(s)^2} \le 1. \tag{9.1}$$

Each norm uses $k_{s,v}$. Volume forms and Ricci bounds are unchanged by reparametrization. The stationary ends occur at $v \le -L(s)$ and $v \ge L(s)$. An increasing $L(s)$ lengthens travel through the family; it need not enlarge the cap's metric diameter. [N, Proposition 7.6, equations (7.80)–(7.83)].

For $\theta = \varepsilon^4$, choose $E = \theta/8$, $F = \theta/(64n)$, $\ell_0 = 64n\theta^{-2}$ and $T_0 = e^{\ell_0}$. On $0 < r \le 1$ put

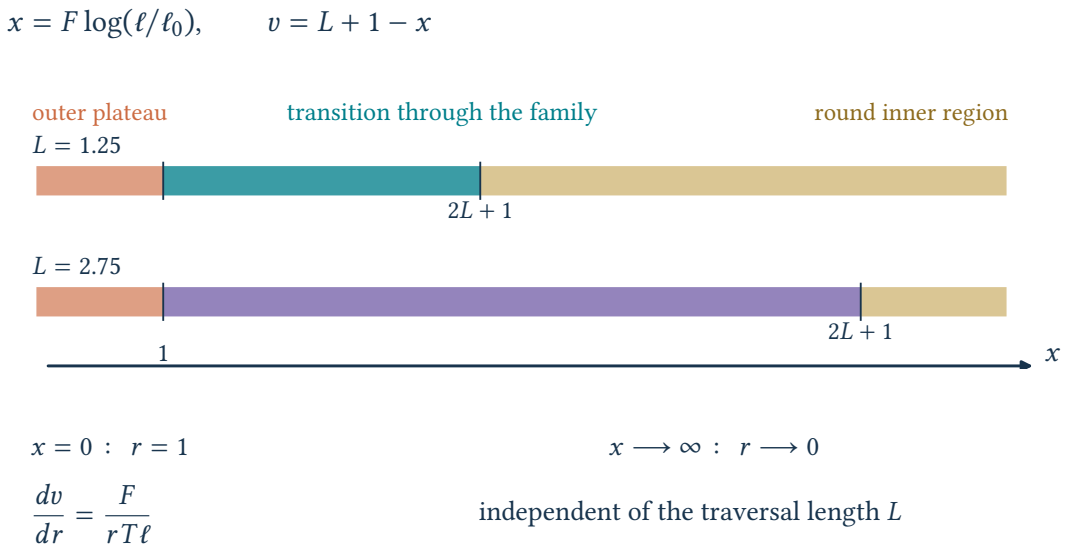
$$T = T_0 - \log r, \quad \ell = \log T, \quad \chi_\varepsilon = 1 - E/\ell, \quad v_{s,\varepsilon}(r) = -F \log \ell + L(s) + 1 + F \log \ell_0.$$

Then $v_{s,\varepsilon}(1) = L(s) + 1$, $v_{s,\varepsilon} \to -\infty$ at zero, and $v_{s,\varepsilon}' = F/(rT\ell) > 0$. Substitution of $k_{s,v_{s,\varepsilon}(r)}$ into the full radial Ricci estimates uses the uniform bound (9.1). The numerical constants of these estimates do not depend on $s$. In particular the weighted first and second derivatives and the weighted mixed Ricci component are bounded by $\varepsilon^4$. The equation $v_{s,\varepsilon}(r_-) = -L(s)$ has a unique smooth solution with nonzero radial derivative. It provides an exact round inner region; there is also an exact stationary outer region. These are the data used in Section 8. [N, equations (7.84)–(7.89)]. Visual K shows how a longer parameter traversal fits deeper within the same radial interval.




Longer parameter travel; uniformly controlled derivatives.

VISUAL J. The slowdown bound as an exact algebraic plot: $A_{\mathrm{maj}} = B + 1$, $a_1 = 4$, $a_2 = 16$, $c_\rho = 16$ satisfy the stated sufficient conditions. The derivative bound remains small while traversal length grows. These are illustrative coefficient bounds, not a selected function $B(s)$ or a specified stationary step. No uniform $s$-derivative bound is asserted.




VISUAL K. The exact clock coordinate $x = F\log(\ell/\ell_0)$ separates the outer plateau, the transition and the round inner region at $x = 1$ and $x = 2L + 1$. Increasing $x$ decreases $r$. A longer traversal fits deeper into the same radial interval, while $dv/dr$ is independent of $L$. Bars show transformed intervals for illustrative $L$, not radial lengths or volumes.

At a seam, equality of boundary metrics makes a continuous piecewise smooth tensor. Positivity of the sum of the second fundamental forms supplies the favourable derivative jump. The gluing proof first fixes a sufficiently small interpolation width $\delta$, and then chooses a mollification width $\nu$ with $8\nu < \delta$ below a threshold depending on that fixed $\delta$. It preserves a specified strictly weaker Ricci

bound and is unchanged away from the collar. Local lower-semicontinuous admissibility thresholds admit smooth positive minorants on a locally finite parameter cover. The construction patches *scalar widths*, not positive-Ricci metrics by convex averaging. [N, Propositions 7.2–7.4].

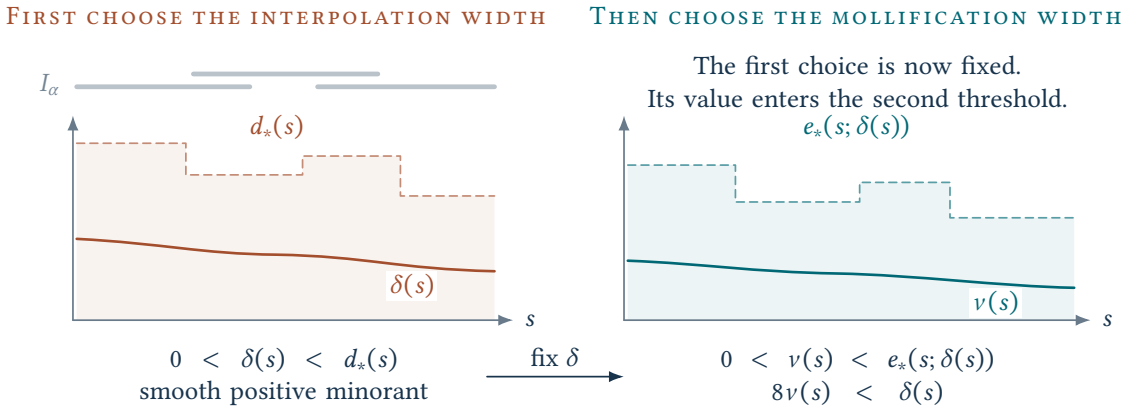
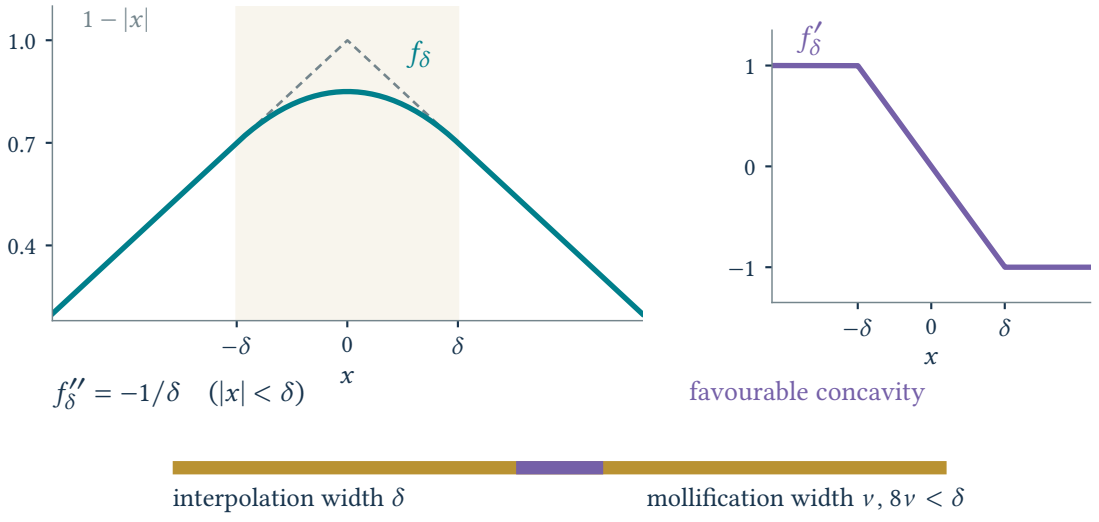



FIGURE 10. Interpolation and mollification widths are chosen in order. The second threshold depends on the first choice; $8\nu < \delta$. Smooth scalar minorants fit local strict margins, with no positive lower bound for the widths on the whole parameter half-line. This explains parameter selection, not by itself the uniform size estimates.



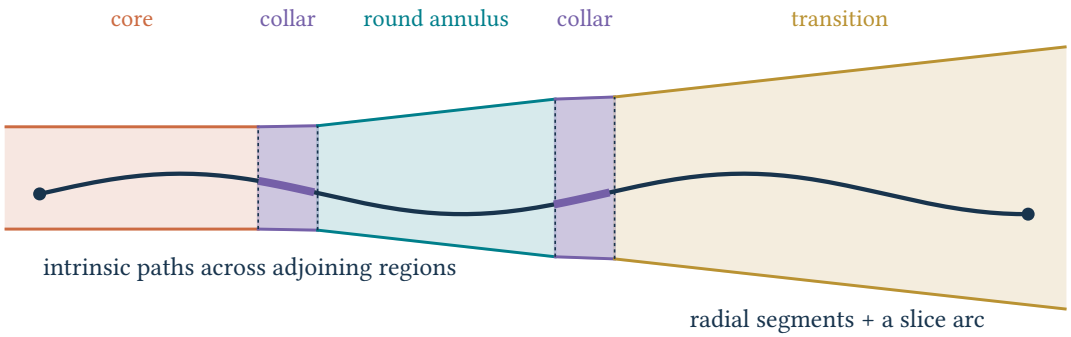

VISUAL L. A scalar $C^1$ interpolation of the favourable jump: replace $1-|x|$ on $[-\delta,\delta]$ by $f_\delta = 1 - \delta/2 - x^2/(2\delta)$. Values and first derivatives match at both ends. Its concavity survives convolution with a nonnegative smooth kernel supported in $[-\nu,\nu]$, with $8\nu < \delta$. This sign model illustrates the ordered widths; it does not replace the tensor Ricci estimates.

To see the uniform metric size, work before the homothety $c_\varepsilon^2$. The transition has warping coefficient at most $r \le 1$ and slice diameter at most $\pi$. Two radial segments and an outer slice arc give diameter at most $2+\pi$, while its volume is bounded by the fixed upper bound for the slice volumes.

The round annulus and scaled core have sizes $O(b)$ and volumes $O(b^n)$, with $b < 1$. A smoothing collar with product comparison constant 2 obeys

$$\operatorname{diam}^{\mathrm{int}} C \le 2\big(w + \operatorname{diam}(\Sigma, h_\Sigma)\big), \qquad \operatorname{Vol} C \le 2^n w \operatorname{Vol}(\Sigma, h_\Sigma).$$

Here its width $w$ and boundary radius are both $O(b)$. If a core path enters the changed collar, replace its first-to-last passage by an intrinsic collar path; the retained portions have exactly the old metric. This bounds distances even though a collar has been modified. The transition, the two collars, the round annulus and the core form a connected chain of regions. Adding their diameter and volume bounds yields constants $D_0$, $V_0$ independent of $s$. Since $c_\varepsilon \le 8\varepsilon$, the final bounds are $8D_0\varepsilon$ and $8^n V_0 \varepsilon^n$. No uniform bound on the unmodified path's derivatives in $s$ was used. [N, Proposition 7.6, pp. 65–66].




$D_0 : \sum$ regional intrinsic diameter bounds

$V_0 : \sum$ regional volume bounds

$c_\varepsilon \le 8\varepsilon \implies \operatorname{diam} \le 8D_0\varepsilon, \qquad \operatorname{Vol} \le 8^n V_0 \varepsilon^n$

Visual M. Five adjoining regions give uniform intrinsic bounds. Paths cross the core, first collar, round annulus, second collar and transition in this order; a modified collar passage is replaced by a controlled intrinsic path. Adding regional diameter and volume bounds gives $D_0$, $V_0$ independent of $s$. The final homothety gives the displayed bounds. Cross-sections and paths are schematic, not an embedding or volume diagram.

Relative and equivariant choices supply a different kind of control: exact agreement. On an initial interval where the input is constant, use the same majorant, Hodge operator, flow initial condition, normal collars, cutoffs and reference seam widths. Perform the two seams in order, on nested parameter intervals on which the previous step already equals the reference construction. The collar-straightening maps are chosen relatively as well. Uniqueness of the Moser flow then makes the terminal collar pullback identical to its reference value. The result is equality of metrics on the same fixed $P_Q$, not merely an isometry between unspecified copies. Transport all these choices through the fixed copy map for the opposite cap. This retains reflection symmetry without averaging Ricci-positive metrics. [N, Proposition 7.6, equations (7.102)–(7.105)].

## 10. The volume surplus pays for the curvature error

*The errors must be small relative to a surplus that also tends to zero.*

The raw capped family has, for sufficiently small $\varepsilon$,

$$\begin{aligned} \mathrm{Ric}_{\widehat{G}(s,\varepsilon)} &> (n-1-A_{\mathrm{Ric}}\varepsilon^2)\widehat{G}(s,\varepsilon), \\ |\operatorname{Vol}(\widehat{G}(s,\varepsilon)) - \gamma(s)\sigma_n| &\le A_{\mathrm{vol}}\varepsilon^n, \\ \operatorname{diam}^{\mathrm{int}} E^{\pm}_{s,\varepsilon} &\le A_{\mathrm{diam}}\varepsilon. \end{aligned}$$

The first bound incorporates the chosen outer seam loss. The second compares the common unchanged band and the four small polar regions; it does not assume that a replacement preserves volume. These are the bounds in [N, equations (8.9)–(8.11)]. Put

$$\beta(s) = \gamma(s)/q - 1 > 0, \qquad d_n(\beta) = (n-1)\big[1-(1+\beta/2)^{-2/n}\big].$$

This $\beta$ is the relative *volume* excess, not the edge parameter $\beta_e$ of Section 5. For the degenerating portion of the path, it is enough to require

$$A_{\mathrm{Ric}}\varepsilon(s)^2 < d_n(\beta(s)), \qquad A_{\mathrm{vol}}\varepsilon(s)^n < \tfrac{1}{2}q\sigma_n\beta(s), \qquad A_{\mathrm{diam}}\varepsilon(s) \longrightarrow 0. \tag{10.1}$$

Then, using $\gamma = q(1+\beta)$,

$$\operatorname{Vol}(\widehat{G}_s) \ge q\sigma_n(1+\beta(s)/2), \tag{10.2}$$

$$\mathrm{Ric}_{\widehat{G}_s} \ge (n-1)(1+\beta(s)/2)^{-2/n}\widehat{G}_s. \tag{10.3}$$

The shared factor in these two estimates is designed, not automatic.

A smooth scale satisfying all these inequalities is obtained by a scalar minorant. The manuscript takes

$$\rho(s) = \min\left\{\varepsilon_0, \varepsilon_*, \frac{1}{1+s}, \sqrt{\frac{d_n(\beta(s))}{2A_{\mathrm{Ric}}}}, \left(\frac{q\sigma_n\beta(s)}{2A_{\mathrm{vol}}}\right)^{1/n}, \frac{1}{(1+s)A_{\mathrm{diam}}}\right\}.$$

Every entry is positive and continuous. On a locally finite interval cover with compact closures choose constants $r_j > 0$ with $4r_j < \inf_{U_j}\rho$ and a smooth subordinate partition of unity $\varphi_j$. Then

$$\varepsilon_\infty(s) = \sum_j \varphi_j(s)r_j \quad \text{satisfies} \quad 0 < \varepsilon_\infty(s) < \rho(s)/4.$$

In particular the curvature loss is smaller than $d_n(\beta)/32$, the volume error is smaller than $q\sigma_n\beta/(2\cdot 4^n)$, and the intrinsic polar diameters tend to zero. This is stronger than merely $\varepsilon(s) \to 0$: the errors must be dominated while $\beta(s) \to 0$. [N, Theorem 8.1, pp. 75–76].

The initial seed is handled separately, because it was fixed before the target $q$. Choose a round initial link of volume fraction $\gamma_*$ and a fixed reference capped metric $\widehat{G}_*$, with volume $V_*$ and Ricci coefficient at least $\lambda_* = (n-1)/4$. It is reflection invariant. The compact filling argument of Section 16 supplies a closing scale $c_Q$. Choose $q_0 < \gamma_*/2$ so small that

$$\begin{aligned} (n-1)\left(1+\frac{\gamma_*/q_0 - 1}{2}\right)^{-2/n} &< \lambda_*, \\ (q_0\sigma_n/V_*)^{2/n} &\le c_Q^2, \\ C_*\varepsilon_*^n &< \tfrac{1}{2}(\gamma_* - q_0)\sigma_n. \end{aligned}$$

The reference construction has already made $C_*\varepsilon_*^n < \gamma_*\sigma_n/8$, so the last requirement leaves a positive range for $q_0$. These inequalities give (10.2)–(10.3) throughout the initial transition and keep its final scaling within the closable range. They are the separate roles of [N, equations (8.6)–(8.8)].

On the initial plateau of the sphere path, the relative construction gives the exact identity $\widehat{G}(s,\varepsilon) = \widehat{G}_\varepsilon$. One smooth scale moves the reference cap size from $\varepsilon_*$ to $\varepsilon_{\mathrm{join}}$; another moves from $\varepsilon_{\mathrm{join}}$ to $\varepsilon_\infty(s)$.

They are both constant and equal to $\varepsilon_{\mathrm{join}}$ near the joining parameter. Thus their resulting metric families agree on an open overlap. This defines a single smooth $\widehat{G}_s$, constant near zero and equal there to the seed. No interpolation between two unrelated positive-Ricci tensors is needed. [N, equation (8.12) and its use in Theorem 8.1].

Now define

$$b_s^n = \frac{q\sigma_n}{\mathrm{Vol}(M_Q, \widehat{G}_s)}, \qquad g_s^0 = b_s^2 \widehat{G}_s.$$

The total volume of $g_s^0$ is exactly $q\sigma_n$. Constant scaling does not change the covariant Ricci tensor, and (10.2) gives $b_s^2 \le (1+\beta/2)^{-2/n}$. Therefore

$$\mathrm{Ric}_{g_s^0} = \mathrm{Ric}_{\widehat{G}_s} \ge (n-1)(1+\beta/2)^{-2/n}\widehat{G}_s \ge (n-1)g_s^0.$$

The two-sided volume-error estimate and $\beta(s) \to 0$ imply $b_s \to 1$. The raw links converge to compact $L_{n,q}$ and hence have bounded diameter for large $s$. The identity correspondence between their metrics before and after scaling has distortion at most $|1-b_s|\,\mathrm{diam}(M_Q, \widehat{G}_s) \to 0$. Thus normalization preserves the limiting metric link. [N, Theorem 8.1, equation (8.18)].

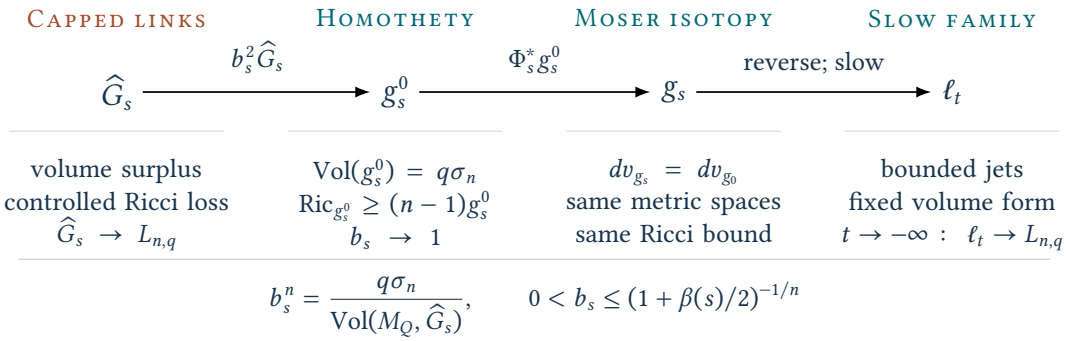
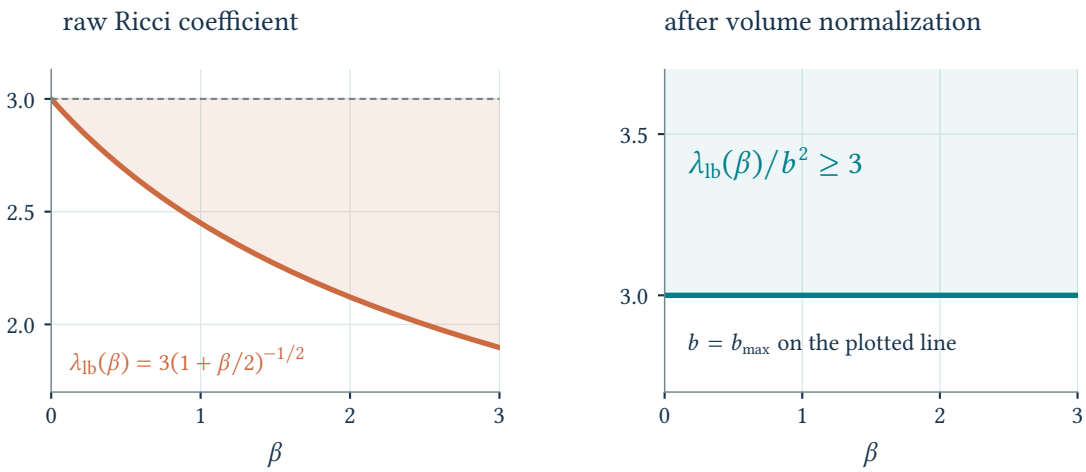



FIGURE 11. Three transformations of the family. Homothety fixes the total volume and the Ricci coefficient; Moser pullback fixes the volume form; reversal and slowdown control derivatives. The $\beta$ here is the relative volume excess. Pullback preserves intrinsic metric spaces, whereas reparametrization changes their speed along the family.




The covariant Ricci tensor stays fixed; its metric coefficient improves.

Visual N. Exact compensation for $n = 4$. Write $\lambda_{\mathrm{lb}}(\beta) = 3(1+\beta/2)^{-1/2}$ for the guaranteed lower raw Ricci coefficient and $b_{\max} = (1+\beta/2)^{-1/4}$. The plotted normalized lower envelope is $\lambda_{\mathrm{lb}}/b_{\max}^2 = 3$; actual normalization has $b \leq b_{\max}$ and therefore $\lambda_{\mathrm{lb}}/b^2 \geq 3$. These are algebraic lower bounds, not measured eigenvalues. Homothety preserves the covariant Ricci tensor.

## 11. A fixed volume form removes a dangerous trace

*Re-identify the same metric spaces before differentiating them.*

The previous section fixed the integral of the volume form on $M_Q$. Now fix the form itself. Put $\omega_s = dv_{g_s^0}$ and use a background Hodge Green operator to define

$$\eta_s = d^*\mathcal{G}\dot{\omega}_s, \qquad \iota_{Y_s}\omega_s = -\eta_s.$$

Since $\int_{M_Q} \dot{\omega}_s = 0$, the Hodge identity gives $d\eta_s = \dot{\omega}_s$. For the flow $\Phi_s$ with $\Phi_0 = \mathrm{id}$,

$$\frac{d}{ds}\Phi_s^*\omega_s = \Phi_s^*(\dot{\omega}_s + d\iota_{Y_s}\omega_s) = 0.$$

A smooth time-dependent vector field on the compact $M_Q$ has a flow on every finite $s$-interval. Uniqueness makes these flows agree on overlaps, giving one family for all $s \geq 0$; a uniform bound over the entire half-line is unnecessary. The field vanishes on the initial constant interval. Thus

$$g_s = \Phi_s^* g_s^0, \qquad dv_{g_s} = dv_{g_0}, \qquad g_0 = g_0^0,$$

with the same Ricci bound, isometry classes and Gromov–Hausdorff limit. [N, Theorem 8.1, p. 78]; [M].

For any smooth radial family $g(r)$ with fixed volume form,

$$\partial_r dv_g = \tfrac{1}{2}\,\mathrm{tr}_g(g')\,dv_g \quad \Longrightarrow \quad \mathrm{tr}_g\, g' = 0, \qquad \mathrm{tr}_g\, g'' = |g'|_g^2.$$

The second identity follows by differentiating the first and using $(g^{-1})' = -g^{-1}g'g^{-1}$. It is not a second vanishing trace. The shape of the slice still changes and still has a radial curvature cost.

Two exact models clarify the distinction. At one tangent space, $g_t = \mathrm{diag}(e^{2t}, e^{-2t})$ has determinant one, $\mathrm{tr}_{g_t}\dot{g}_t = 0$, and $|\dot{g}_t|_{g_t}^2 = 8$. On $\mathbb{R}/\mathbb{Z}$, the densities $\rho_a(x) = 1 + a\sin(2\pi x)$, $|a| < 1$, have integral one. Their cumulative coordinate

$$F_a(x) = x + \frac{a}{2\pi}(1 - \cos(2\pi x))$$

has $F_a' = \rho_a > 0$ and $F_a(x+1) = F_a(x) + 1$. For $\Phi_a = F_a^{-1}$, $\rho_a(\Phi_a(u))\Phi_a'(u) = 1$. This fixes the density by pullback, not by changing its integral.

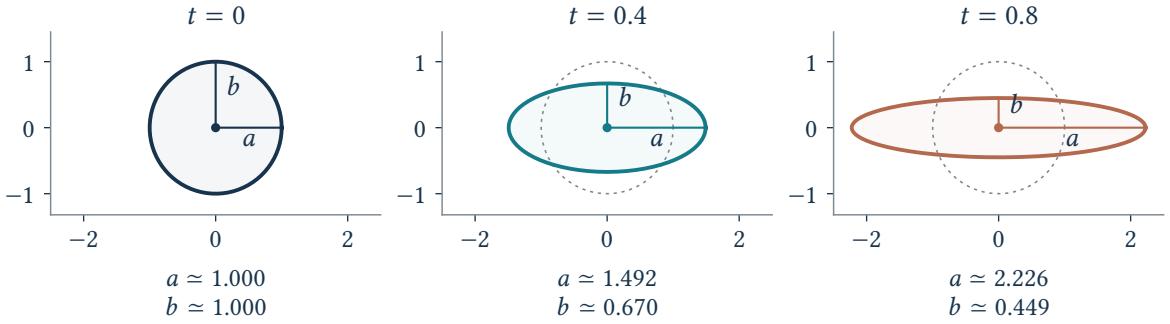



FIGURE 12. The ellipses $\mathrm{diag}(e^t, e^{-t})(S^1)$ all enclose area $\pi$. Their semiaxes are the eigenlengths of $g_t = \mathrm{diag}(e^{2t}, e^{-2t})$; the metric unit balls have reciprocal semiaxes. This is a pointwise matrix model, not a positive-Ricci metric family on a sphere.

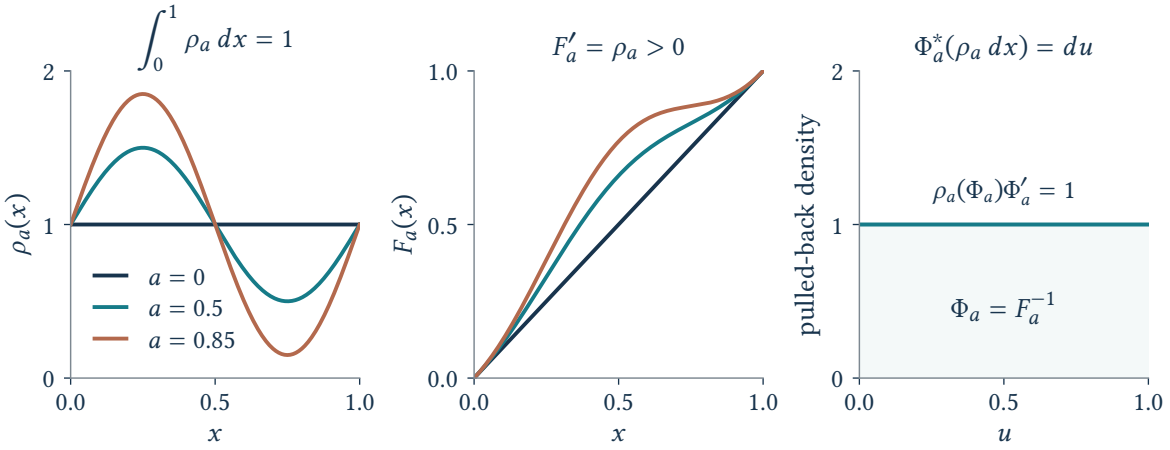



FIGURE 13. Equal integrals do not imply equal densities. The inverse cumulative-coordinate map pulls $\rho_a\,dx$ back to $du$ exactly. This circle model illustrates the volume-form operation used on the higher-dimensional closed manifold.

Reverse the family, using $g_{-t}$ for $t \le 0$ and $g_0$ for $t \ge 0$. Stationarity near the join makes this smooth. The subsequent slowdown must leave a reserve for the return paths in Section 17. Here is the explicit selection used in [N, Proposition 9.2]. For $j \ge 0$, let $A_j$ bound one plus the three required derivative norms on the original parameter interval $[-j-2, -j+1]$. Choose smooth functions $\vartheta, \xi : [0,1] \to [0,1]$, constant near each endpoint, with

$$\vartheta(0) = \xi(0) = 0, \qquad \vartheta(1) = \xi(1) = 1, \qquad \vartheta' \ge 0.$$

Use $\vartheta$ for the slowdown and $\xi$ for the return in Section 17; extend both constantly beyond $[0,1]$. Fix $C_0 \ge 1$ such that

$$\|\vartheta'\|_\infty + \|\vartheta''\|_\infty + \|\xi'\|_\infty + \|\xi''\|_\infty \le C_0,$$

and put

$$C_{\mathrm{cut}} = 3(1 + 2C_0) + (1 + 2C_0)^2 + 2C_0, \qquad \eta_0 = \min\{1/2, (2C_{\mathrm{cut}})^{-1}\}.$$

Choose lengths $L_j \geq 1$ with

$$\frac{2C_0A_j}{L_j} + \frac{(C_0 + C_0^2)A_j}{L_j^2} \leq \eta_0.$$

Map consecutive intervals of lengths $L_j$ smoothly onto $[-j-1, -j]$, using the stationary cutoff. Their lengths sum to infinity, so they cover the negative half-line and still reach every sufficiently negative original parameter. Endpoint constancy makes the assembled reparametrization smooth. The chain rule yields, for the slowed family denoted from now on by $\ell_t$,

$$\|\dot{\ell}_t\|_{\ell_t} + \|\ddot{\ell}_t\|_{\ell_t} + \|\nabla^{\ell_t}\dot{\ell}_t\|_{\ell_t} \leq \eta_0 \leq 1. \tag{11.1}$$

It retains $dv_{\ell_t} = dv_{g_0}$, $\mathrm{Ric}_{\ell_t} \geq (n-1)\ell_t$, $\ell_t = g_0$ for $t \geq 0$, and $(M_Q, \ell_t) \to L_{n,q}$ as $t \to -\infty$.

## 12. The Ricci cost of moving the link

*Concavity supplies radial curvature; the full tensor must still be positive.*

Consider the metric

$$G = dr^2 + w(r)^2 g(r), \qquad w(r) = rh(r), \qquad g(r) = \ell_{f(r)}.$$

Let $A_r = g^{-1}g'$ and $\lambda_w = w'/w$. The slice shape operator is $S = \lambda_w I + A_r/2$. The common volume form gives $\operatorname{tr} A_r = 0$, so

$$\operatorname{tr} S = n\lambda_w, \qquad \operatorname{tr}(S^2) = n\lambda_w^2 + \tfrac{1}{4}|g'|_g^2.$$

The normal Ricci formula gives

$$\mathrm{Ric}_G(\partial_r, \partial_r) = -n\frac{w''}{w} - \frac{1}{4}|g'|_g^2. \tag{12.1}$$

Thus concavity supplies a positive term, while movement of the link costs curvature. The mixed block involves $\nabla g'$ and the tangential block involves $g''$; this explains all three norms in (11.1). The complete formulas and their estimates are in [N, Proposition 6.2]. The radial strategy follows [CN].

Use the induced slice metric $\widehat{g}(r) = w(r)^2 g(r)$ for the block comparison. If $e$ is $g(r)$-unit, then $w^{-1}e$ is $G$-unit. Suppose

$$\mathrm{Ric}_G(\partial_r, \partial_r) \geq \alpha > 0, \qquad \mathrm{Ric}_G|_{TM_Q} \geq \gamma\widehat{g} \quad (\gamma > 0), \qquad |\mathrm{Ric}_G(\partial_r, \cdot)|_{\widehat{g}} \leq b.$$

For $V$ tangent to the slice, write $|V| = |V|_{\widehat{g}} = |V|_G$. Then

$$\mathrm{Ric}_G(x\partial_r + V, x\partial_r + V) \geq \alpha x^2 - 2b|x||V| + \gamma|V|^2.$$

These are the full-metric unit-frame conventions of [N, Proposition 6.2, equations (6.13)–(6.22)]. In particular, the coefficient $\gamma$ below is not a lower bound expressed in unrescaled coordinate components of $g$. Completing the square, or taking the determinant of the corresponding two-by-two matrix, shows that $\alpha\gamma > b^2$ suffices for positivity in *every* direction. Positive diagonal components alone do not suffice. Figure 14 illustrates the loss of positivity; Visual O places the construction's normalized bound on the positive side of the same threshold.

## 13. A clock slow enough for every small annulus

*Infinite parameter travel is compatible with vanishing movement per scale.*

For $0 < r \leq 1$, the dimension-only choice in [N, Lemma 9.1] is

$$E = \frac{1}{16}, \quad F = \frac{1}{128(n+1)}, \quad L_0 = 64(n+1), \quad T_0 = e^{L_0}, \quad \rho = e^{-T_0},$$

$$T = -\log(\rho r) = T_0 - \log r, \qquad L = \log T, \qquad h = 1 - \frac{E}{L}, \qquad f = -F\log L + F\log L_0.$$

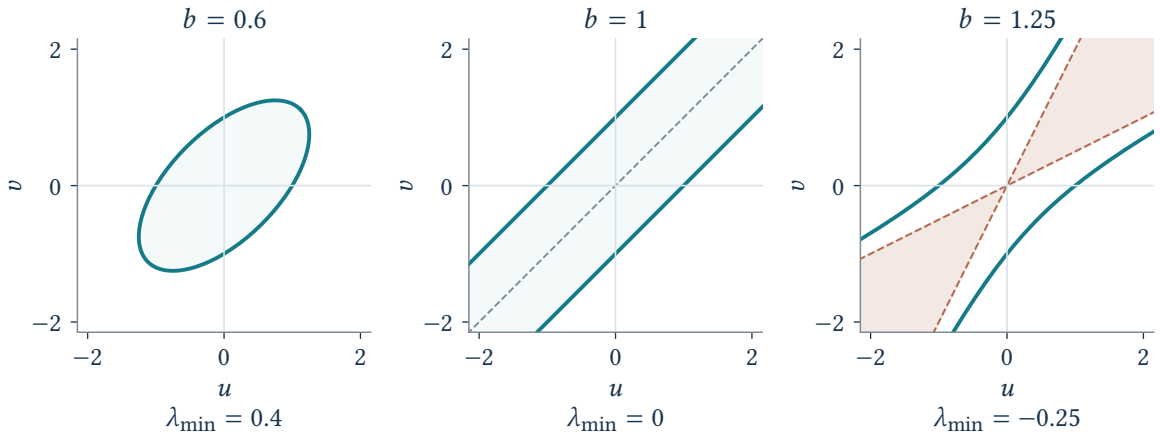



FIGURE 14. The conics $Q_b = u^2 - 2buv + v^2 = 1$ have eigenvalues $1 \pm b$. They are an ellipse for $b = 0.6$, parallel lines for $b = 1$, and a hyperbola for $b = 1.25$. Negative-value regions illustrate how an uncontrolled mixed term defeats positive diagonal coefficients.

Direct differentiation gives

$$rf' = \frac{F}{TL}, \qquad h' = -\frac{E}{rTL^2},$$
$$w' = 1 - \frac{E}{L} - \frac{E}{TL^2}, \qquad w'' = -\frac{E}{rTL^2} - \frac{E}{rT^2L^2} - \frac{2E}{rT^2L^3}.$$

Consequently $h \to 1$, $f \to -\infty$, $rf' \to 0$, and $w' \to 1$ as $r \downarrow 0$. Also $1/2 < w' < 1$ and $w'' < 0$ on this region. The parameter travels infinitely far, but its variation over every fixed multiplicative radial interval tends to zero.

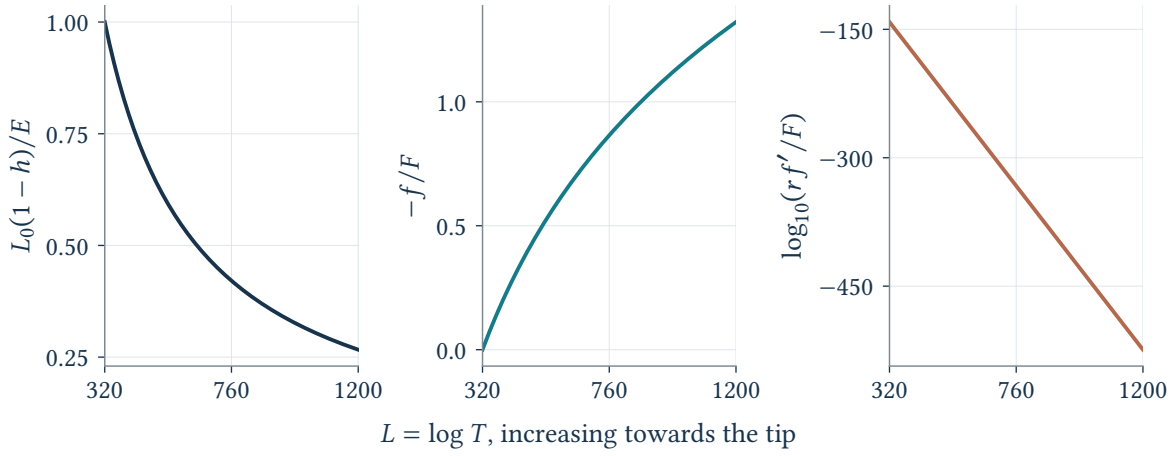



FIGURE 15. The actual radial clock for $n = 4$, with $E = 1/16$, $F = 1/640$, $L_0 = 320$ and $\rho = \exp(-\exp 320)$. Increasing $L$ approaches the tip. The scaled curves show $h \to 1$, $f \to -\infty$ and $rf' \to 0$ without numerically evaluating the extremely small radial scales.

The component bounds supplied by [N, Proposition 6.2 and Lemma 9.1] are

$$\alpha = \frac{E}{2L^2Tr^2}, \qquad \gamma = \frac{E}{Lr^2}, \qquad b = \frac{\sqrt{n}F}{LTr^2}.$$

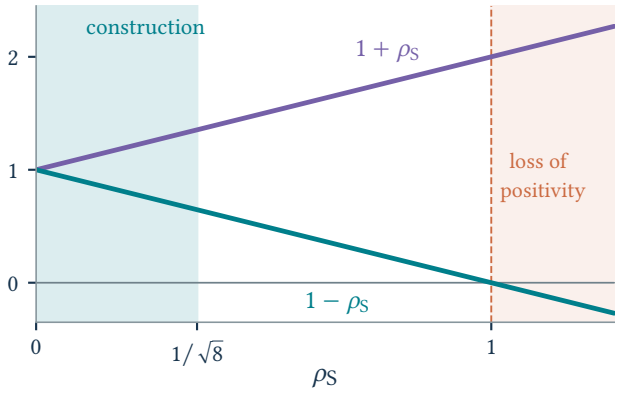
Their mixed-cost ratio is

$$\frac{b^2}{\alpha\gamma} = \frac{2nF^2L}{E^2T} \le \frac{1}{8},$$

because $E \ge 2\sqrt{nF}$ and $T/L \ge 4$. This proves positive Ricci curvature in the varying region once the stated component estimates are inserted. At $r = 1$ the parameter reaches zero and the link becomes constant. The warping is extended by integrating a nonnegative compactly supported truncation of $-w''$, chosen to have total mass less than $w'(1)$. It remains smooth, increasing and concave, is eventually linear, and has $0 < w' < 1$. The parameter extends smoothly and increasingly with positive values for $r > 1$. The constant-link formulas give $\mathrm{Ric} \ge 0$ there. No changing-link term is discarded before the family becomes stationary. [N, Lemma 9.1, pp. 80–81].

A common scale exposes the mixed term

$$X = \sqrt{\alpha}\,|x|, \quad Y = \sqrt{\gamma}\,|V|, \quad \rho_S = b/\sqrt{\alpha\gamma}$$




$$Q = X^2 - 2\rho_S XY + Y^2$$

$$Q \ge (1-\rho_S)(X^2+Y^2)$$

$$\rho_S^2 \le \frac{1}{8}$$

The construction stays strictly inside the positive-definite region.

Visual O. With $|V| = |V|_G$, $X = \sqrt{\alpha}|x|$ and $Y = \sqrt{\gamma}|V|$, the mixed-term lower bound becomes $Q = X^2 - 2\rho_S XY + Y^2$. Its normalized comparison matrix has eigenvalues $1 \pm \rho_S$. The radial construction gives $\rho_S^2 \le 1/8$, leaving a positive margin. The shaded strip records this sufficient bound; the matrix is not the entire Ricci tensor.

## 14. The completion remembers the fixed manifold

*The radial coordinate becomes distance from the added point.*

Bonnet–Myers applied to $\mathrm{Ric}_{\ell_t} \ge (n-1)\ell_t$ gives $\mathrm{diam}(M_Q, \ell_t) \le \pi$. The intrinsic slice diameter is therefore at most $\pi w(r) \to 0$. For $0 < r \le s$, a radial segment and a curve in the radius-$r$ slice give

$$d_G((r,x),(s,y)) \le s - r + \pi w(r).$$

All sequences with radii tending to zero thus define the same completion point $p$. Conversely, $r$ is 1-Lipschitz, since $|dr|_G = 1$. A Cauchy sequence with positive limiting radius lies in a compact positive-radius cylinder, where the smooth tensor induces the product topology; it converges there. A Cauchy sequence cannot have unbounded radial coordinate. Exactly one point is added.

Radial paths and the lower Lipschitz bound now give the identity

$$d(p,(r,x)) = r. \tag{14.1}$$

The inclusion of the original punctured Riemannian length space into its completion is isometric. Thus its Riemannian distance is the ambient distance restricted from $Y$, including distances approximated by paths approaching the tip.

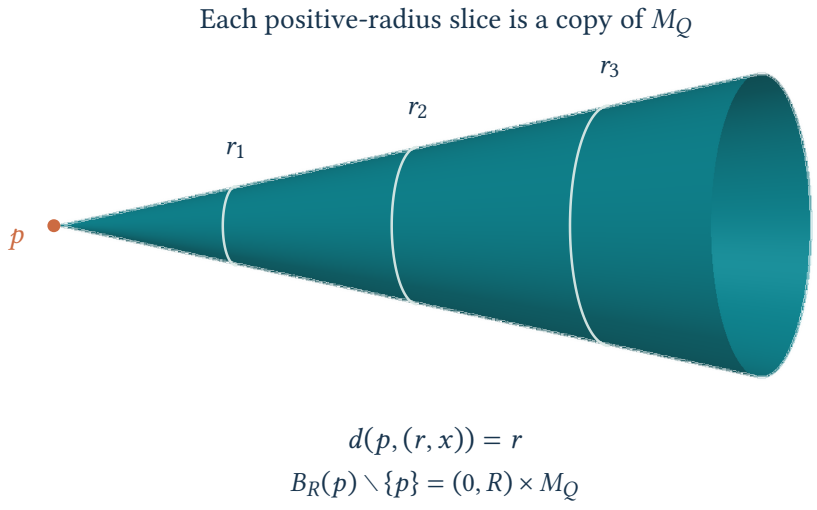



FIGURE 16. Each positive-radius slice is a copy of the fixed manifold $M_Q$. Its shrinking diameter gives one completion point with $d(p,(r,x)) = r$. The rings denote entire $n$-manifolds; the picture records radial organization rather than an embedding.

The map from the closed topological cone $([0,R] \times M_Q)/(\{0\} \times M_Q)$ to $\overline{B}_R(p)$, given by the radial coordinates, is a continuous bijection. It is continuous at the vertex by (14.1); away from the vertex both topologies are the product topology. Compactness of the domain and the Hausdorff property of the target make it a homeomorphism. Thus $Y$ is proper as well as complete. Restricting to the open radius-$R$ cone gives the asserted local homeomorphism. The completed space is a length space; compactness of bounded balls and Arzelà–Ascoli applied to nearly minimizing curves give minimizing geodesics. These properties justify the distance comparisons below. [N, Proposition 9.2, pp. 82–83].

## 15. WHY EVERY BLOW-UP GIVES THE SAME CONE

*First compare ambient annular distances, then include the vertex.*

Rescale by $r = \lambda t$. On a fixed annulus the tensor is

$$\lambda^{-2} G = dt^2 + t^2 h(\lambda t)^2 \ell_{f(\lambda t)}.$$

For $0 < a < b < \infty$, integrating $f'$ gives

$$\sup_{a \le t \le b} |f(\lambda t) - f(\lambda)| \le \max\{|\log a|, |\log b|\} \sup_{\min(a,1)\lambda \le r \le \max(b,1)\lambda} |r f'(r)| \longrightarrow 0.$$

For a fixed nonzero tangent vector $V$, the derivative bound implies $|\partial_u \log \ell_u(V,V)| \le 1$. Hence

$$e^{-|u-v|} \ell_v \le \ell_u \le e^{|u-v|} \ell_v.$$

Together with $h(\lambda t) \to 1$, this compares the rescaled annular tensor with the cone tensor having frozen link $\ell_{f(\lambda)}$. The frozen links converge to $L_{n,q}$ because $f(\lambda) \to -\infty$. [N, equations (9.12)–(9.13)].

Here is the passage from tensors to ambient distances. Fix $0 < \alpha < b$. On $[\alpha/2, 2b]$ write the tensor comparison factors as $e^{\pm\delta_\lambda}$, where $\delta_\lambda \to 0$, and let $\eta_\lambda = e^{\delta_\lambda/2} - 1$. For endpoints with radial coordinates in $[\alpha, b]$, put $S = r_z + r_{z'} \le 2b$. Both distances are at most $S$ by the path through the vertex. A minimizing curve cannot reach radius greater than $2b$, since its radial variation alone would exceed that bound. If it enters radius less than $\alpha/2$, its length is at least $S - \alpha$. If it avoids that region, the tensor comparison applies to its full length. Applying these alternatives to minimizers in both spaces gives

$$|d_{\lambda^{-2}G}(z,z') - d_{\text{frozen cone}}(z,z')| \le 2\alpha + 2b\,\eta_\lambda. \tag{15.1}$$

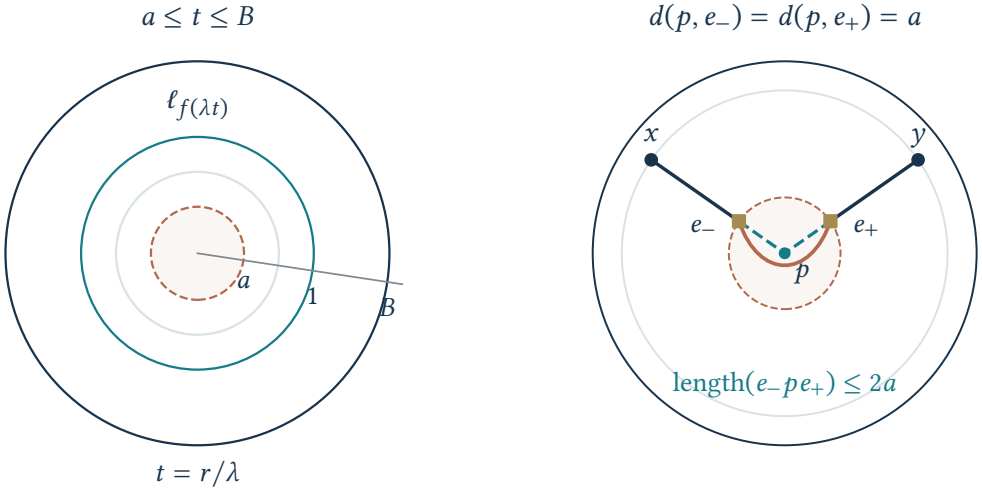



FIGURE 17. The tensor comparison is annular, whereas the distances are ambient. Replacing an entire inner passage by a radial route through the vertex costs at most twice the small inner radius. The curves do not presume that minimizers remain in the annulus.

Thus the comparison does not inadvertently replace ambient distances by intrinsic annulus distances. [N, equation (9.14)].

Choose a correspondence between the frozen link and $L_{n,q}$ with distortion $\varepsilon_\lambda \to 0$. Relate cone points at the same radius using this correspondence. The cone formula, the 1-Lipschitz map $s \mapsto \min\{s, \pi\}$, $|\cos x - \cos y| \le |x - y|$, and $|\sqrt{x} - \sqrt{y}| \le \sqrt{|x - y|}$ give distortion at most $\sqrt{2}\, b\, \sqrt{\varepsilon_\lambda}$ on the radius-$b$ cone ball. Compose on the annulus with (15.1); then relate every point of either closed radius-$\alpha$ inner ball to the other vertex. Both projections are surjective and the vertex pair is retained.

For two outer pairs the composed estimate applies. For an inner pair and an outer pair of common outer radius $t$, the triangle inequality shows that the distance in the space containing the inner point differs from $t$ by at most $\alpha$; in the other space the vertex distance is exactly $t$. Two inner pairs contribute at most $2\alpha$, including when their nonvertex points lie in opposite factors. Thus these extra pairs introduce no larger error. The resulting closed-ball correspondence has distortion at most

$$2\alpha + 2b\eta_\lambda + \sqrt{2}\, b\, \sqrt{\varepsilon_\lambda}.$$

First let $\lambda \downarrow 0$ with $\alpha, b$ fixed, then let $\alpha \downarrow 0$. This proves pointed convergence at all scales, not just along one selected sequence:

$$(Y, \lambda^{-1} d, p) \longrightarrow \mathrm{C}(L_{n,q}).$$

The tangent cone is therefore unique. [N, Proposition 9.2, p. 84].

## 16. The initial metric supplies a smooth filling

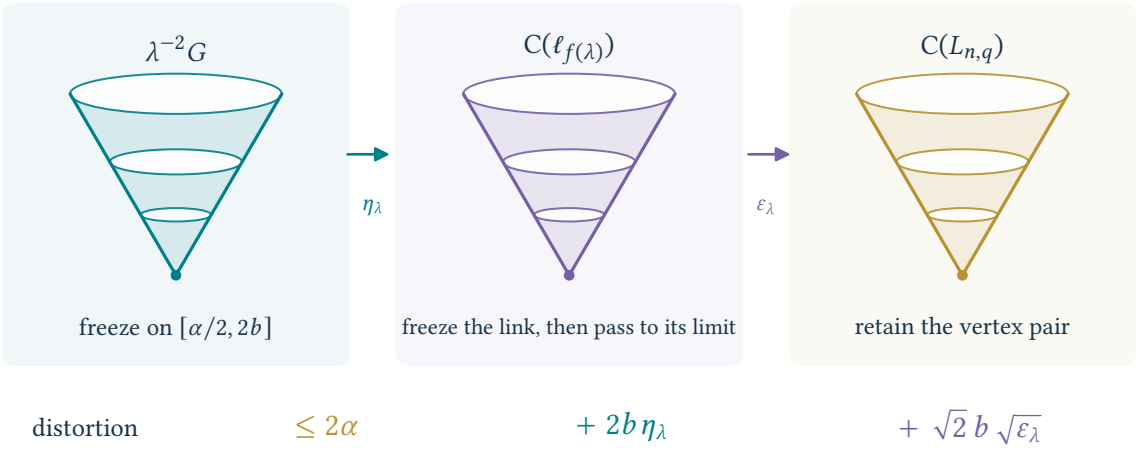
*An exact conical end does not impose a basepoint-distance coordinate.*

In [N, Definition 2.2], $g_0$ is Ricci closable if, for every $0 < \eta < 1$, a complete connected smooth boundaryless Ricci-nonnegative $(n+1)$-manifold has a compact connected smooth domain $K_\eta$, an interior basepoint, and exterior tensor exactly

$$([1, \infty) \times M_Q,\ dR^2 + R^2(1 - \eta) g_0).$$

The compact domain need not be a metric ball. The coordinate $R$ is not required to be distance from the basepoint. The smooth-tensor identity, including a collar of its inner boundary, is the datum used below.

The reflection-symmetric raw seed $\widehat{G}_*$ has positive Ricci curvature, and reflection fixes its equatorial hypersurface, whose normal bundle is trivial. The construction in [R, proof of Proposition 3.2] supplies




VISUAL P. The all-scale argument separates three errors: discarding a small inner region, comparing ambient distances with the frozen-link cone, and passing from the frozen link to $L_{n,q}$. The displayed distortion bound is for a pointed surjective correspondence of closed radius-$b$ balls. The wedges record radial coordinates and whole links, not embeddings or intrinsic-annulus distances.

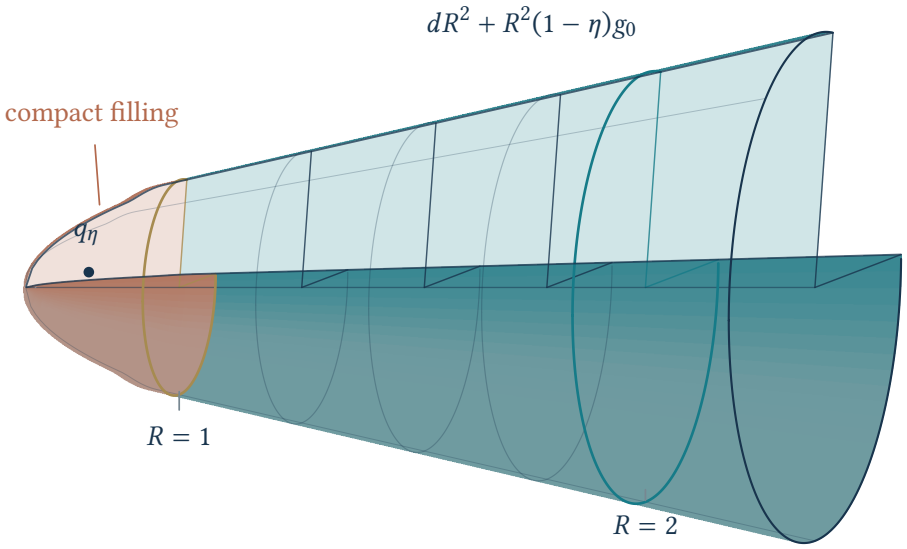



FIGURE 18. A compact filling with exact conical end. The coordinate $R$ labels the end and need not be the distance from the interior basepoint. No uniform diameter bound for the compact filling is part of closability.

a compact positive-Ricci filling with convex boundary isometric to this prescribed metric; the relevant compact-filling input is used in [N, Theorem 8.1]. Retain the boundary-connected component and normalize its boundary to $\widehat{G}_*$. Write its inward-convention boundary form as at least $\kappa_{\mathrm{fill}}\widehat{G}_*$ and its boundary metric's Ricci bound as $\mathrm{Ric}_{\widehat{G}_*} \geq \lambda_*\widehat{G}_*$. This is an external geometric existence input, not a conclusion from the schematic filling picture.

The subsequent exact-end attachment can be described directly. Choose

$$2c_Q < \kappa_{\mathrm{fill}}, \qquad 4(n-1)c_Q^2 < \lambda_*.$$

For $0 < \eta < 1$ put $a = c_Q\sqrt{1-\eta}$. Take a smooth decreasing cutoff $\chi$ on $[0,\infty)$ with $\chi(0) = 1$, $\chi' = 0$ to all orders at its terminal support point 1, and $\chi' < 0$ on $[0,1)$. One choice is $\chi(t) = e^{-t/(1-t)}$ for $t < 1$ and zero for $t \geq 1$. Define

$$F_\eta(t) = 1 + a\int_0^t (1+\chi(s))\,ds.$$

Then $F_\eta(0) = 1$, $F_\eta'(0) = 2a$, $a \leq F_\eta' \leq 2a$, and $F_\eta'' \leq 0$, strictly below zero near the seam. The cylinder $dt^2 + F_\eta(t)^2\widehat{G}_*$ has radial Ricci $-nF_\eta''/F_\eta \geq 0$ and tangential Ricci at least

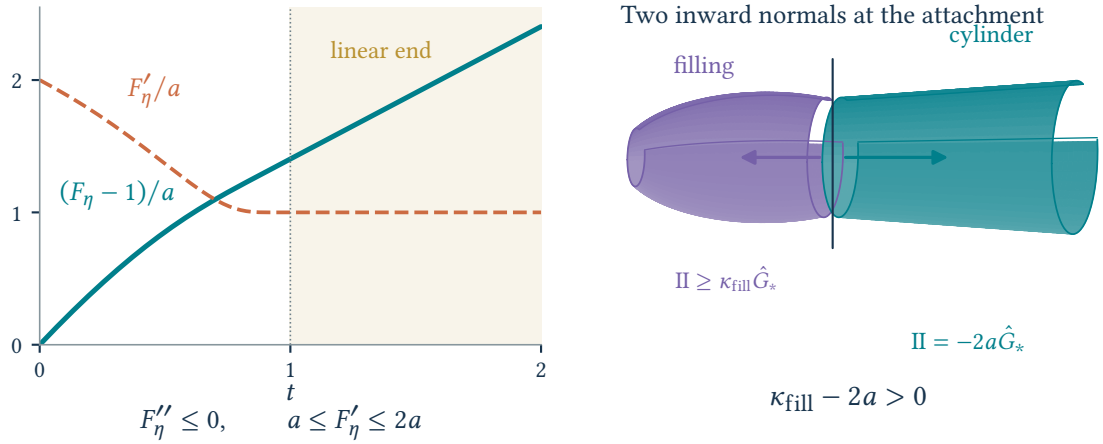
$$\frac{\lambda_* - 4(n-1)c_Q^2}{F_\eta(t)^2} > 0.$$

At its inner boundary it contributes $-2a\widehat{G}_*$, so the sum with the filling form is positive. Smoothing in a small collar retains positive Ricci there and leaves the end untouched. For $t \geq 1$, $F_\eta(t) = at + c$; using $R = t + c/a$ makes the tensor exactly

$$dR^2 + R^2(1-\eta)c_Q^2\widehat{G}_*.$$

Starting this end at a positive coordinate and then homothetically normalizing that starting coordinate gives Definition 2.2. Compact sublevel sets of an extended radial function prove completeness. [N, Theorem 8.1, pp. 71–72].

### A controlled opening reaches an exactly linear end




For $t \geq 1$: $F_\eta = at + c$, so $R = t + c/a$ gives the exact cone tensor.

> Visual Q. The specified cutoff gives the plotted dimensionless warp and slope; the end is exactly linear for $t \geq 1$. The inward normals explain the opposite boundary-form signs and their positive sum. The shaded pieces are dimension-suppressed fibre diagrams, not an embedded realization of the filling metric.

The seed and $c_Q$ are fixed *before* $q_0$. The choice in Section 10 gives $b_0^2 = (q\sigma_n/V_*)^{2/n} \leq c_Q^2$. Closability is preserved by scaling a link down: if $g$ is closable and $0 < a \leq 1$, then for $0 < \eta < 1$ choose $\eta' = 1 - a^2(1-\eta) \in (0,1)$; the end with cross-section $(1-\eta')g$ is exactly the one needed for $(1-\eta)a^2 g$. Applying this to $a = b_0/c_Q$ proves that $g_0 = b_0^2\widehat{G}_*$ is closable. The later Moser flow is the

identity initially, so it does not change this seed. This is why the argument does not assume that every member of the degenerating family, or an arbitrary normalized link, is closable. [N, Theorem 8.1, p. 78].

## 17. Return to the closable metric near the tip

*Each smooth approximation uses only a finite portion of the degeneration.*

For $m \geq 2$, set $a_m = 1 - 1/m$ and use the endpoint-constant cutoff $\xi$ chosen before (11.1). Define

$$c_m(t) = \begin{cases} 0, & t \leq -2m, \\ t\xi((t+2m)/m), & -2m \leq t \leq -m, \\ t, & t \geq -m, \end{cases} \qquad k_t^{(m)} = a_m \ell_{c_m(t)}.$$

The path is smooth, returns to $a_m g_0$ for $t \leq -2m$, and agrees with $a_m \ell_t$ on every fixed parameter interval for all sufficiently large $m$. For fixed $m$ its volume form is $a_m^{n/2} dv_{g_0}$, independent of $t$, and $\mathrm{Ric}_{k_t^{(m)}} \geq (n-1)k_t^{(m)}$.

The derivative reserve is explicit. The cutoff bounds give

$$\|c_m'\|_\infty \leq 1 + 2C_0, \qquad \|c_m''\|_\infty \leq 2C_0.$$

A covariant two-tensor obeys $|a_m T|_{a_m g} = |T|_g$, whereas a covariant three-tensor obeys $|a_m S|_{a_m g} = a_m^{-1/2}|S|_g \leq \sqrt{2}|S|_g$. Thus the sum of the three derivative norms of $k_t^{(m)}$ is at most

$$\eta_0\left(3\|c_m'\|_\infty + \|c_m'\|_\infty^2 + \|c_m''\|_\infty\right) \leq 1.$$

The same dimension-only functions $h, f$ therefore apply to all these returned paths. Uniformity here would not follow from separate slowdowns that changed $h, f$ with $m$. [N, Proposition 9.2, equations (9.15)–(9.16)].

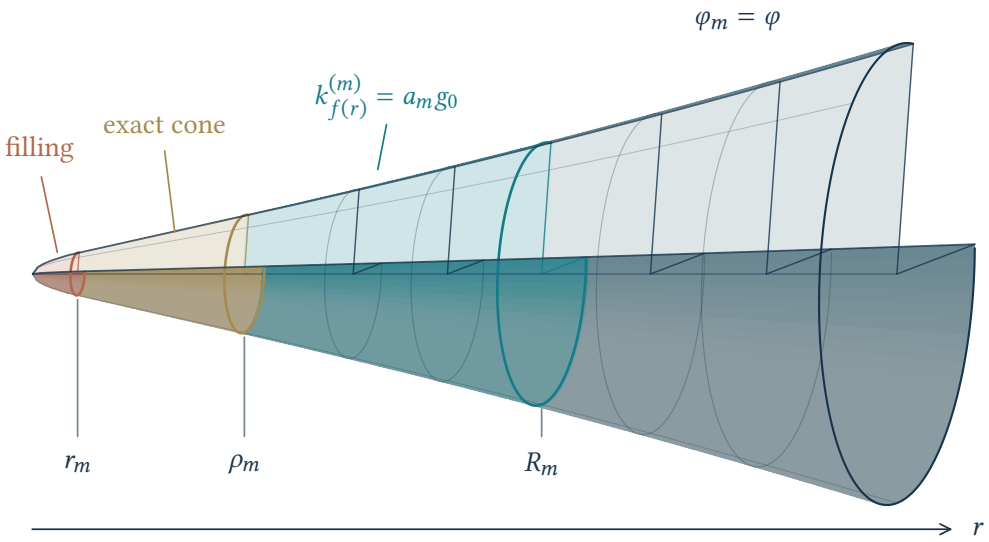
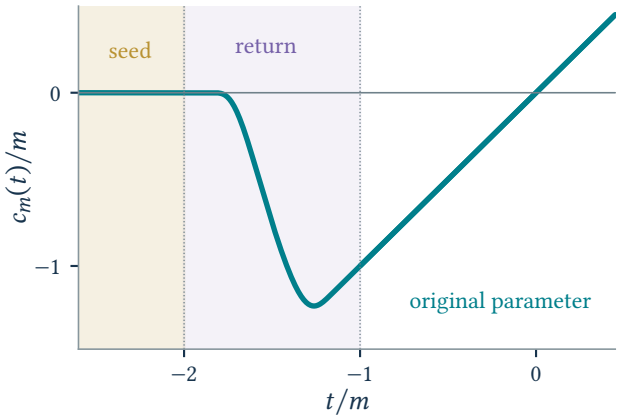



Figure 19. Radial zones in a smooth approximation. Below $R_m$ the link has returned to $a_m g_0$; the warping becomes exactly linear below $\rho_m$. The filling is inserted at $r_m < \rho_m$. The original warping resumes at $R_m$, while a link-return transition may continue farther out.

One derivative reserve serves every returned path




$$k_t^{(m)} = a_m \ell_{c_m(t)}$$

$$|a_m T|_{a_m g} = |T|_g$$

covariant rank two

$$|a_m S|_{a_m g} = a_m^{-1/2} |S|_g$$

covariant rank three; $a_m^{-1/2} \le \sqrt{2}$

The reserved bound $\eta_0$ absorbs both the cutoff derivatives and this scaling cost.

VISUAL R. The return parameter is constant at the seed, turns through a finite portion of the family, and then agrees with the original parameter. The plot uses a representative smooth endpoint-constant cutoff and is not monotone on the return interval. The tensor-norm identities are exact; the rank-three cost explains why the initial slowdown must leave a fixed reserve for every $m$.

Choose $R_m \downarrow 0$ with $f(R_m) < -2m$ and $R_m < 1/m$. The strict inequality and continuity make the link constant on a neighbourhood of $R_m$. Section 18 constructs a concave $\varphi_m$, equal to $\varphi = rh$ for $r \ge R_m$, and equal to $d_m r$ for $r \le \rho_m$, with $0 < d_m < 1$ and $d_m \to 1$. Its inner tensor is exactly

$$dr^2 + r^2 b_m g_0, \qquad b_m = a_m d_m^2 \in (0,1), \qquad b_m \to 1.$$

On the constant-link region the mixed Ricci term vanishes. The radial term is $-n\varphi_m''/\varphi_m \ge 0$; the tangential term on a normalized direction is at least

$$\varphi_m^{-2}\left(\frac{n-1}{a_m} - \varphi_m\varphi_m'' - (n-1)(\varphi_m')^2\right) \ge 0,$$

since $\varphi_m'' \le 0$ and $0 < \varphi_m' \le 1$. Outside that region the original varying-link estimate applies. At $R_m$ the warping jets agree and the link is constant on an open overlap. Consequently the whole punctured approximation is smooth and Ricci nonnegative, and converges smoothly to $G$ on every compact positive-radius cylinder. [N, equations (9.17)–(9.19)].

## 18. A MOMENT IDENTITY MAKES THE INNER CONE FIT

*Preserve value and slope while retaining concavity.*

Put $\kappa = -\varphi'' > 0$ near zero. The limits $\varphi(r)/r \to 1$ and $\varphi'(r) \to 1$ imply

$$\int_0^R \kappa = 1 - \varphi'(R) < \infty, \qquad \varphi(R) = R - \int_0^R (R-t)\kappa(t)\,dt.$$

Choose $0 < \alpha < \beta < \gamma < R$, a smooth $0 \le \chi \le 1$ equal to one near zero and supported in $[0,\alpha)$, and let $M_0 = \int \chi\kappa > 0$, $M_1 = \int t\chi\kappa > 0$. Take $\zeta \ge 0$ smooth, supported in $(\beta,\gamma)$, with $\int t\zeta = M_1$. Then

$$\int \zeta \le M_1/\beta < M_0,$$

because $M_1 < \alpha M_0$. Moving the first moment outward reduces the required total mass. Set

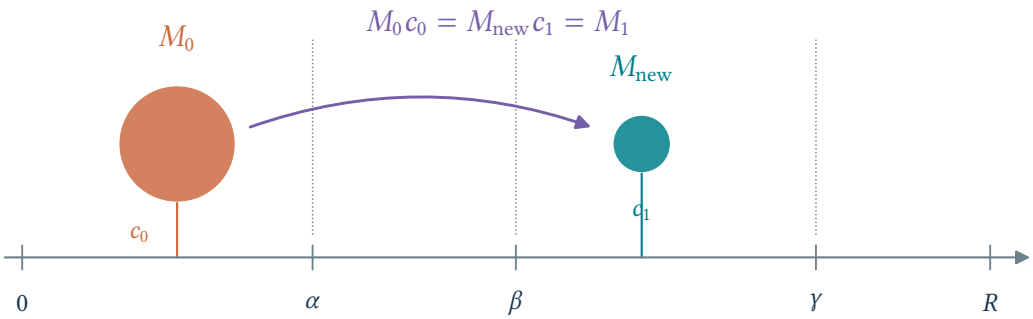
$$\kappa_R = (1-\chi)\kappa + \zeta, \quad d_R = 1 + \int_0^R (\kappa_R - \kappa), \quad \varphi_R(r) = d_R r - \int_0^r (r-t)\kappa_R(t)\,dt. \tag{18.1}$$

Near zero $\kappa_R = 0$, so $\varphi_R = d_R r$ exactly. At $R$,

$$\varphi_R'(R) - \varphi'(R) = d_R - 1 - \int_0^R (\kappa_R - \kappa) = 0,$$
$$\varphi_R(R) - \varphi(R) = \int_0^R t(\kappa_R - \kappa)(t)\,dt = 0.$$

Since $\kappa_R = \kappa$ near $R$, value and slope matching imply equality on a neighbourhood of $R$, including all jets. Extend by $\varphi$ beyond $R$.

Move the same first moment outward with less mass




$$c_0 < \alpha < \beta < c_1 \quad \Longrightarrow \quad M_{\text{new}} < M_0$$

$d_R = 1 + M_{\text{new}} - M_0 < 1$: the lost mass is absorbed by the initial slope.

Visual S. Each disk represents a nonnegative curvature measure by its total mass and centroid, not by its spatial density. The removed measure $\chi\kappa\,dt$ has centroid $c_0 = M_1/M_0 < \alpha$; the inserted measure $\zeta\,dt$ has centroid $c_1 = M_1/M_{\text{new}} > \beta$. Equal first moments therefore require less inserted mass. The disk areas use illustrative centroid values; the displayed identities are exact.

Nonnegativity of $\kappa_R$ gives concavity and

$$\varphi_R'(r) \geq \varphi_R'(R) = \varphi'(R) > 0, \qquad \varphi_R'(r) \leq d_R < 1 \quad (0 \leq r \leq R).$$

Also $0 < 1 - d_R \leq 1 - \varphi'(R) \to 0$, so $d_R > 0$ for small $R$ and $d_R \to 1$. The modified second derivative is smooth even though the original $\kappa$ need only be integrable at zero: it has been removed identically on a whole interval there. These observations prove the properties used in Section 17. [N, Proposition 9.2, pp. 85–86].

Visual S gives the general mass-and-centroid mechanism. The following scalar example, illustrated in Figures 20–21, can be read separately.

*A reproducible scalar example.* On $[0,1]$, take $\varphi = r - 0.3r^2$ and $\kappa = 0.6$. Let

$$S(u) = \frac{e^{-1/u}}{e^{-1/u} + e^{-1/(1-u)}} \quad (0 < u < 1),$$

extended by zero and one outside this interval, and set $\chi(r) = 1 - S((r - 0.10)/0.15)$. The identity $S(1 - u) = 1 - S(u)$ gives $M_0 = 0.6 \int_0^1 \chi = 0.105$ exactly. Let $b(u) = e^{-1/(1-u^2)}$ for $|u| < 1$, zero otherwise, and $Z = \int_{-1}^1 b$. With $M_1 = \int_0^1 0.6 r\chi(r)\, dr$, put

$$\zeta(r) = \frac{M_1 b((r - 0.60)/0.10)}{0.60 \cdot 0.10 \cdot Z}.$$

Evenness of $b$ gives $\int r\zeta = M_1$ and $\int \zeta = M_1/0.60 < M_0$. Formula (18.1) now gives $\varphi_R = d_R r$ for $r \le 0.10$ and $\varphi_R = \varphi$ for $r \ge 0.70$. Its derivative is at least $\varphi_R'(1) = 0.4$. The moment identity is exact; the decimal labels for $M_1$ in the plots are numerical illustrations.

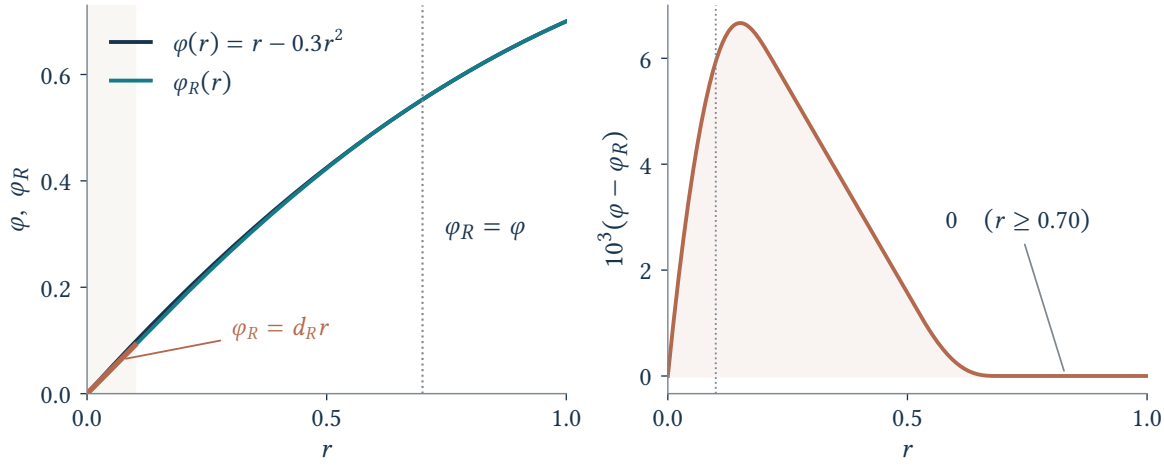



FIGURE 20. The scalar model $\varphi = r - 0.3r^2$ and its concave replacement. The replacement is exactly linear near zero and exactly equal to the original beyond 0.70. The magnified difference locates the change; it is not a numerical proof of exact matching.

## 19. Choose the filling first, then shrink it

*A small boundary does not imply a small interior.*

Apply closability to $\eta_m = 1 - b_m$. If $K_m$ is the compact closing domain, add its exact cone collar through $R = 2$ and denote the resulting compact connected smooth domain by

$$W_m = K_m \cup \Phi_m([1, 2] \times M_Q).$$

Its intrinsic diameter $D_m$ is finite: interior and boundary half-charts give its intrinsic metric the manifold topology, and connectedness and compactness give finite distances and finite diameter. There is no uniform bound on $D_m$ in the input. Choose the insertion scale only after $D_m$ is known:

$$0 < r_m < \min\left\{\rho_m, \frac{1}{m}, \frac{2}{m(1 + D_m)}\right\}, \qquad \tau_m = r_m/2,$$

$$\mathcal{F}_m = (W_m, \tau_m^2 H_m), \qquad \delta_m = \tau_m D_m < 1/m, \qquad e_m = r_m + \delta_m < 2/m.$$

The diameter controlled here is intrinsic. It bounds the length of a path inserted through the filling. [N, Proposition 9.2, pp. 86–87].

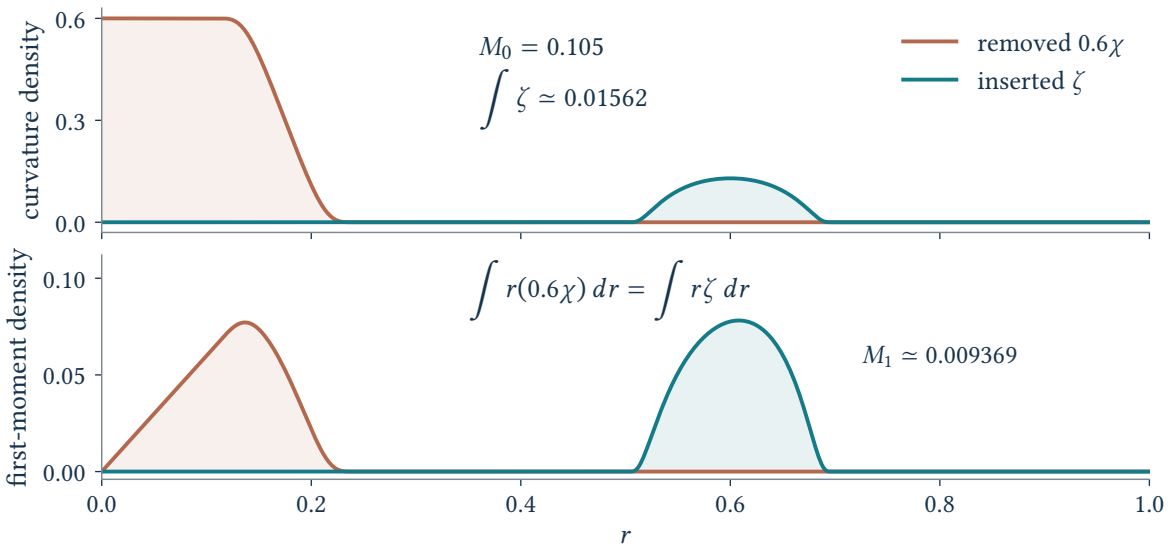



FIGURE 21. The removed and inserted curvature densities. Their first moments agree exactly by normalization of the even bump. The total inserted mass is smaller because its support is farther out. The approximate labels illustrate the integrals in the scalar example.

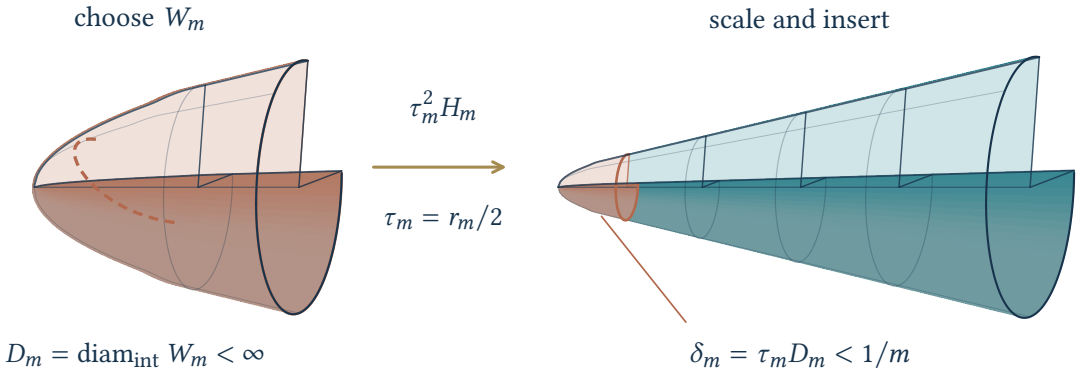



FIGURE 22. Choose the compact filling before measuring $D_m$, then choose $r_m$ and scale by $(r_m/2)^2$. The inserted intrinsic diameter is $\delta_m < 1/m$. The silhouette represents the domain, not a quantitative measurement of its intrinsic diameter.

The original exact-end tensor is valid for $3/2 < R < 5/2$, an open neighbourhood of $\partial W_m$ at $R = 2$. Under $r = (r_m/2)R$, it becomes $dr^2 + r^2 b_m g_0$. Choose

$$0 < \omega_m < \min\{r_m/4, \rho_m - r_m\}.$$

Both sides of the attachment are restrictions of this one smooth tensor on $r_m - \omega_m < r < r_m + \omega_m$. They therefore agree to all normal orders, not just in their boundary values. The identified manifold $(M_m, G_m, p_m)$ is smooth, connected, without boundary, and has $\mathrm{Ric}_{G_m} \geq 0$. [N, equations (9.20)–(9.21)]. Figure 23 records the common tensor on the open overlap; Visual T tracks the homothety and radial change of coordinates.

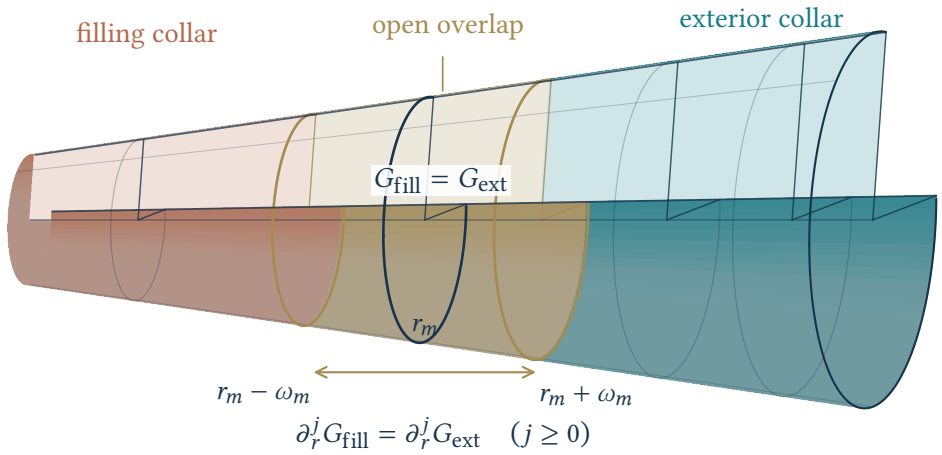
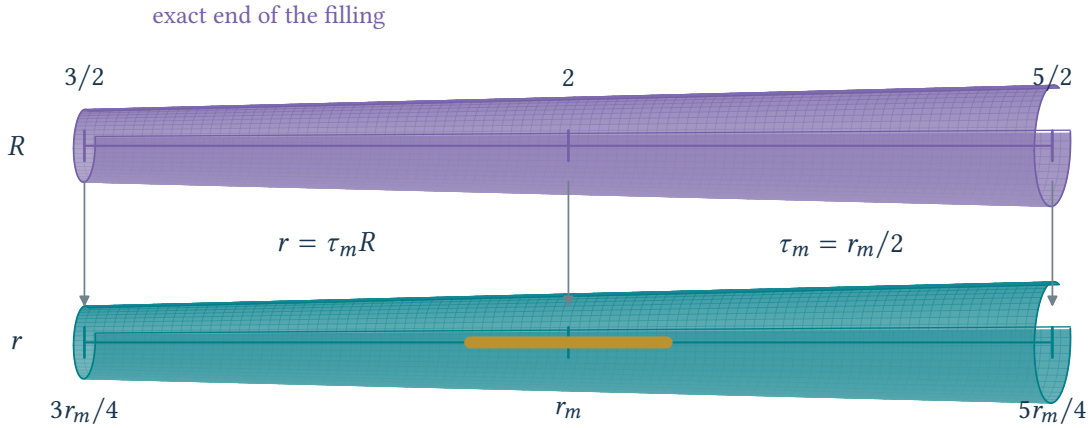



FIGURE 23. The filling and exterior collars agree as one tensor on an open interval about $r_m$. All normal jets agree, so this final attachment requires no new curvature-losing seam smoothing. The cross-sections are $M_Q$, not necessarily round spheres.

A homothety identifies an open collar, including every jet




$|r - r_m| < \omega_m$: both sides equal $dr^2 + r^2 b_m g_0$.

$\omega_m < \min\{r_m/4, \rho_m - r_m\}$

VISUAL T. The exact end is rescaled by $\tau_m^2$, with $r = \tau_m R$ and $\tau_m = r_m/2$. The interval $3/2 < R < 5/2$ maps to $3r_m/4 < r < 5r_m/4$. The smaller highlighted overlap also lies below $\rho_m$, so both restrictions are one smooth tensor there and agree to every normal order. The highlighted width is schematic; cross-sections are the full manifold $M_Q$.

Extend the radial function by the constant $r_m$ on the filling. Near the seam it is the maximum of the collar coordinate and $r_m$; elsewhere it is constant or has differential of norm one. It is therefore globally 1-Lipschitz. A path inside the filling followed by a radial segment gives the other direction of the estimate

$$r - r_m \leq d_{G_m}(p_m, (r, x)) \leq r - r_m + \delta_m, \qquad |d_{G_m}(p_m, (r, x)) - r| \leq e_m. \tag{19.1}$$

Every point of the filling is within $\delta_m$ of $p_m$. The closed based radius-$R$ ball lies in the compact set $\mathcal{F}_m \cup ([r_m, R + r_m] \times M_Q)$. It is closed there, since the smooth metric induces the manifold topology.

All closed bounded balls are compact, which proves properness and completeness. The argument never identifies the filling with a metric ball. [N, equation (9.22)].

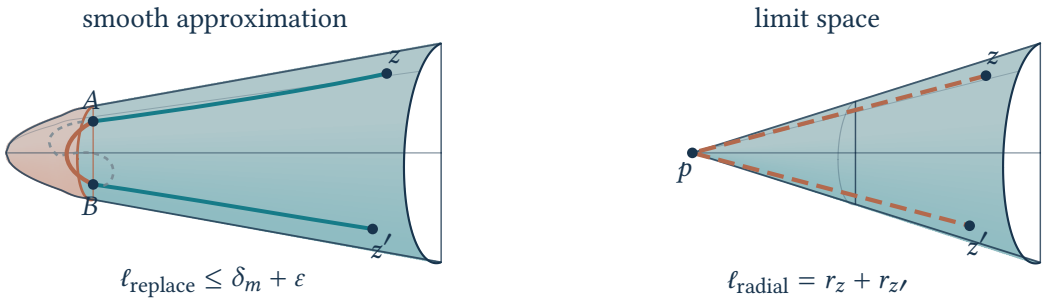



FIGURE 24. The first-to-last passage through a filling can be replaced by an intrinsic path of length arbitrarily close to $\delta_m$. In the limit, radial paths through $p$ have the indicated length. These are controls of shortcuts, not assertions that a given minimizer must be radial.

On every compact positive-radius cylinder, $G_m \to G$ smoothly: eventually the return transition lies below that cylinder, and the remaining slice factor is just $a_m \ell_{f(r)}$, with $a_m \to 1$. To compare ambient distances, fix $0 < \alpha < R$ and take $m$ sufficiently large that $r_m < \alpha/2$ and $\delta_m < R$. On $[\alpha/2, 3R] \times M_Q$, choose $0 < \eta_m < 1$, with $\eta_m \to 0$, such that

$$(1 - \eta_m)G \le G_m \le (1 + \eta_m)G.$$

Set

$$\lambda_m(\alpha, R) = \max\{\sqrt{1 + \eta_m} - 1,\ (1 - \eta_m)^{-1/2} - 1\}.$$

This controls length comparison in both directions and tends to zero. For endpoints with radii in $[\alpha, R]$, put $S = r_z + r_{z'} \le 2R$. Radial paths and the intrinsic filling diameter give $d_{G_m}(z, z') \le S - 2r_m + \delta_m < 3R$; the route through the limiting vertex gives $d_Y(z, z') \le S$. A curve reaching radius $3R$ would have radial variation at least $6R - S \ge 4R$, so a minimizer in either space stays below $3R$.

The inner region is $\mathcal{F}_m \cup ([r_m, \alpha/2] \times M_Q)$ in $M_m$, and the closed radius-$\alpha/2$ ball in $Y$; the former is a coordinate domain, not an asserted based metric ball. If a minimizer enters this region, its length is at least $S - \alpha$. Otherwise its full length is controlled by the common exterior tensors. The two alternatives, applied in each space, give

$$d_{G_m}(z, z') - d_Y(z, z') \le \max\{2R\lambda_m, \alpha + \delta_m\},$$
$$d_Y(z, z') - d_{G_m}(z, z') \le \max\{3R\lambda_m, \alpha\}.$$

Consequently

$$|d_{G_m}(z, z') - d_Y(z, z')| \le \alpha + \delta_m + 3R\lambda_m(\alpha, R). \tag{19.2}$$

A local tensor convergence assertion alone would not establish this ambient-distance estimate. [N, equation (9.23)].

There is one final radius issue. Put $\mathcal{D}_m(R) = \mathcal{F}_m \cup ([r_m, R] \times M_Q)$ with its ambient restricted distance. This is a coordinate domain, not necessarily the actual based ball. Relate identical outer coordinates in $\mathcal{D}_m(R)$ and $\overline{B}^Y_R(p)$; relate all points of $\mathcal{D}_m(\alpha)$ to $p$, and $p_m$ to the inner ball in $Y$. Both projections are surjective and $(p_m, p)$ belongs to the relation. For two outer pairs use (19.2). Two inner pairs have distortion at most $2\alpha + \delta_m$, since points of $\mathcal{D}_m(\alpha)$ can be joined through the filling. For an outer point $w = (r, x)$ and $z \in \mathcal{D}_m(\alpha)$,

$$r - \alpha \le d_{G_m}(z, w) \le r + \alpha + \delta_m,$$

so a mixed pair of this type costs at most $\alpha + \delta_m$. The other mixed type costs at most $\alpha + e_m$, by (19.1) and the triangle inequality in $Y$. These cases give the common bound

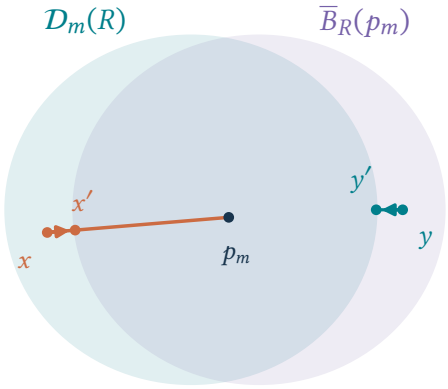
$$\operatorname{dis} C_m(\alpha, R) \le 2\alpha + e_m + 3R\lambda_m(\alpha, R),$$

where $C_m(\alpha, R)$ denotes this correspondence. By (19.1), $\mathcal{D}_m(R)$ lies in the radius-$(R + e_m)$ based ball. A point lying outside the radius-$R$ ball can be moved into it along a minimizing geodesic from $p_m$, over length at most $e_m$. Conversely, a point of the actual ball with coordinate $r > R$ has $r \le R + r_m$ and moves to the coordinate slice $R$ along a radial segment of length at most $r_m$. Points in the filling already belong to $\mathcal{D}_m(R)$. Thus their ambient Hausdorff distance is at most $e_m$. The distance-$e_m$ relation is a pointed surjective correspondence with distortion at most $2e_m$. Composing gives an actual closed-ball correspondence with distortion at most

$$2\alpha + 3e_m + 3R\lambda_m(\alpha, R). \tag{19.3}$$

Let $m \to \infty$, then $\alpha \downarrow 0$. This proves pointed Gromov–Hausdorff convergence to $(Y, d, p)$, with the correct based balls and basepoint pair. [N, Proposition 9.2, pp. 88–89]. Visual U separates the two corrections: minimizing-geodesic trimming for excess based distance and radial trimming for excess coordinate radius.

The last correction replaces a coordinate cutoff by a metric ball




Set diagram in the common ambient space

$x \mapsto x'$ along a based geodesic

$d(x, x') \le e_m$

$y \mapsto y'$ along a radial segment

$d(y, y') \le r_m \le e_m$

$d_H(\mathcal{D}_m(R), \overline{B}_R(p_m)) \le e_m$; the added correspondence costs at most $2e_m$.

Visual U. The coordinate domain and the actual based ball are compared in the same ambient metric. Excess based distance is trimmed along a minimizing geodesic, while excess radial coordinate is trimmed along a radial segment. The resulting Hausdorff bound supplies a pointed surjective correspondence of distortion at most $2e_m$. The overlapping outlines show set membership only, not Euclidean geometry.

## 20. Noncollapse, density, and boundary

*Three conclusions, with three distinct reasons.*

**Based noncollapse.** For large $m$, the fixed annulus $\mathcal{A} = \{1/4 \le r \le 1/2\}$ is in the exterior and lies in $B_1(p_m)$ by (19.1). Smooth convergence there gives

$$\operatorname{Vol}_{G_m}(\mathcal{A}) \longrightarrow \operatorname{Vol}_G(\mathcal{A}) > 0.$$

After discarding finitely many indices, the volumes of the based unit balls have a common positive lower bound. It comes from an unchanged-size annulus, not from a uniform size of the shrinking filling. [N, Proposition 9.2].

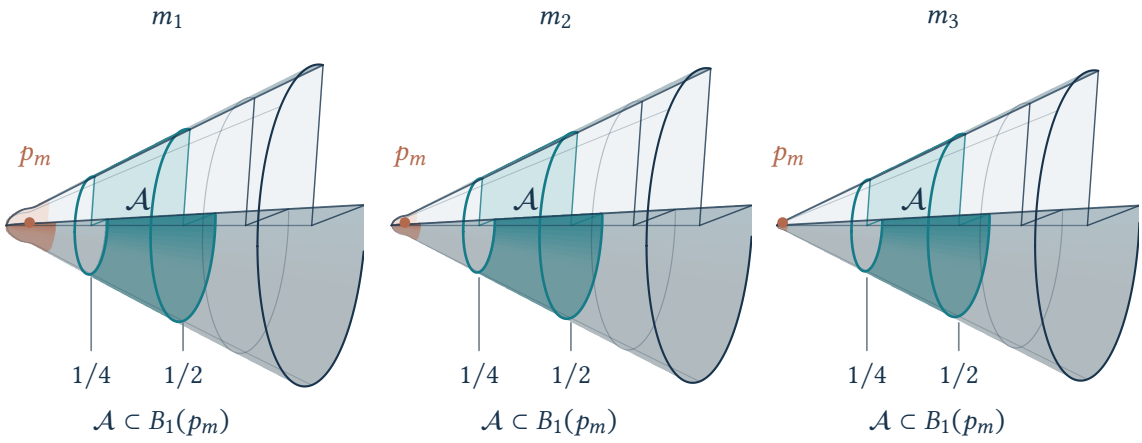



FIGURE 25. The fixed annulus eventually lies in the based unit ball and has volume tending to a positive limit. Its volume supplies noncollapse while the inserted filling shrinks. The panels are qualitative stages of the realizing sequence.

**Density at the tip.** Normalize Hausdorff measure to equal smooth Riemannian volume. Away from $p$, the ambient distance is locally the smooth Riemannian distance; the singleton has zero $N$-dimensional measure. Since the slices have common volume $q\sigma_n$ and $d(p,(r,x)) = r$,

$$\mathcal{H}^{n+1}(B_r(p)) = q\sigma_n \int_0^r t^n h(t)^n \, dt = q\omega_{n+1} r^{n+1} + o(r^{n+1}).$$

For example, the error after division by $q\omega_{n+1} r^{n+1}$ is bounded in absolute value by $\sup_{0<t<r} |h(t)^n - 1| \to 0$. This computes the density as $q$ without a rate for convergence of the links. [N, §10].

For the illustrative choice $n = 4$, $h(r) = 1 - 0.15r$ on $[0,1]$, binomial expansion gives

$$\frac{q\sigma_4 \int_0^r t^4(1-0.15t)^4 \, dt}{q\omega_5 r^5} = \sum_{k=0}^{4} \binom{4}{k} (-0.15r)^k \frac{5}{5+k} \longrightarrow 1.$$

This polynomial calculation isolates the integration of slice volumes. The actual radial construction uses the logarithmic $h$ of Section 13.

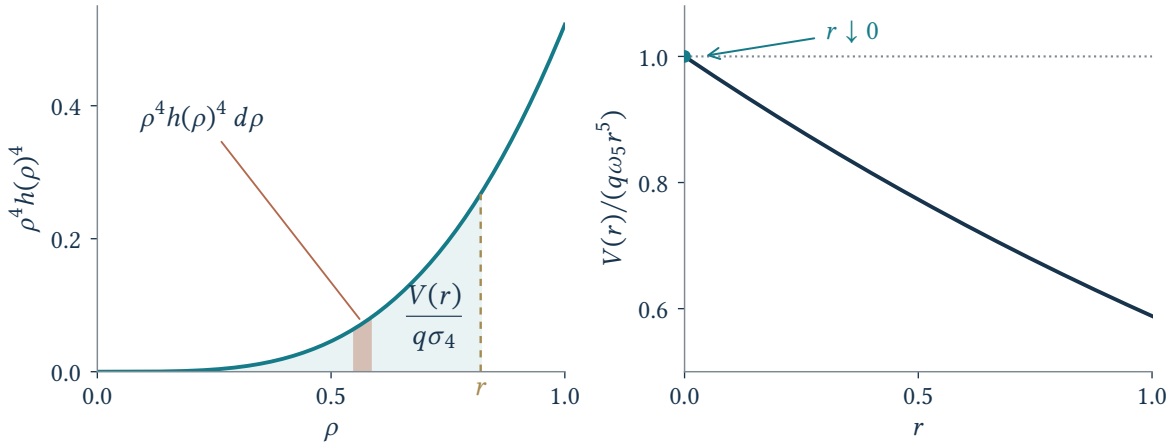



FIGURE 26. The density integral for the illustrative polynomial model. The common factor $q\sigma_4$ is suppressed in the left panel; the normalized integral on the right tends to one. This is not a replacement for the logarithmic radial metric used in the construction.

**Kapovitch–Mondino boundary.** The smooth boundaryless approximants, with $\mathrm{Ric} \geq 0$, are noncollapsed $\mathrm{RCD}(0, N)$ spaces with reference measures $\mathcal{H}^N$. The based volume lower bound rules out the collapsed alternative in [DPG, Theorem 1.2]; the limit measure is $\mathcal{H}^N$. The hypotheses of [KM, Theorem 1.10] are then satisfied: pointed convergence, noncollapse, and topological manifold approximants without boundary. That theorem gives $\partial_{\mathrm{KM}} Y = \emptyset$. This does not imply that the limit is a topological manifold, nor that its local homology is spherical. [N, §2 and §10].

## 21. Local homology retains the vanished caps

*A contractible neighbourhood can still fail to be a manifold neighbourhood.*

Let $U = B_{r_0}(p) \cong \mathrm{C}_{\mathrm{top},r_0}(M_Q)$. Its contraction is $[r, x] \mapsto [(1-t)r, x]$. Compactness of $M_Q$ ensures continuity at the vertex: every neighbourhood of the collapsed fibre contains a full smaller cone, and the contraction preserves it. The puncture retracts onto a radius-$a$ slice by

$$(r, x) \longmapsto ((1-t)r + ta, x), \qquad 0 < a < r_0.$$

Excision identifies $H_j(Y, Y \setminus \{p\}; A)$ with $H_j(U, U \setminus \{p\}; A)$. The reduced exact sequence of this pair, using contractibility of $U$, gives

$$H_j(Y, Y \setminus \{p\}; A) \cong \widetilde{H}_{j-1}(M_Q; A) \quad (j \geq 1). \tag{21.1}$$

For $j = 0$, connectedness and the nonempty puncture make the relative group zero; this agrees with $\widetilde{H}_{-1} = 0$. These are homology groups of a pair, not absolute homology of the contractible cone. [N, §10].

For $n = 4$, $Q = \mathbb{CP}^2$, the usual cell decomposition gives $H_2(Q; \mathbb{Z}) = \mathbb{Z}$. The boundary collar makes $(Q, P_Q)$ a good pair, and $Q/P_Q \cong S^4$. Therefore $H_2(Q, P_Q) = H_3(Q, P_Q) = 0$ and $H_2(P_Q; \mathbb{Z}) \cong \mathbb{Z}$. A collar-adapted open cover of the connected sum has overlap retracting onto $S^3$. Its Mayer–Vietoris sequence contains

$$0 = H_2(S^3) \longrightarrow H_2(P_Q) \oplus H_2(-P_Q) \longrightarrow H_2(M_Q) \longrightarrow H_1(S^3) = 0.$$

Thus $H_2(M_Q; \mathbb{Z}) = \mathbb{Z}^2$ and (21.1) gives $H_3(Y, Y \setminus \{p\}; \mathbb{Z}) = \mathbb{Z}^2$. A point of a $d$-dimensional manifold without boundary has local integral homology $\mathbb{Z}$ in degree $d$ and zero in all other degrees. No $d$ gives $\mathbb{Z}^2$ in degree three. Hence $p$ is a nonmanifold point. Orientation reversal changes orientation data, not the displayed homology groups. All other points are smooth, so $\mathcal{S}_{\mathrm{top}}(Y) = \{p\}$. [N, proof of Corollary 3.3 and §10].

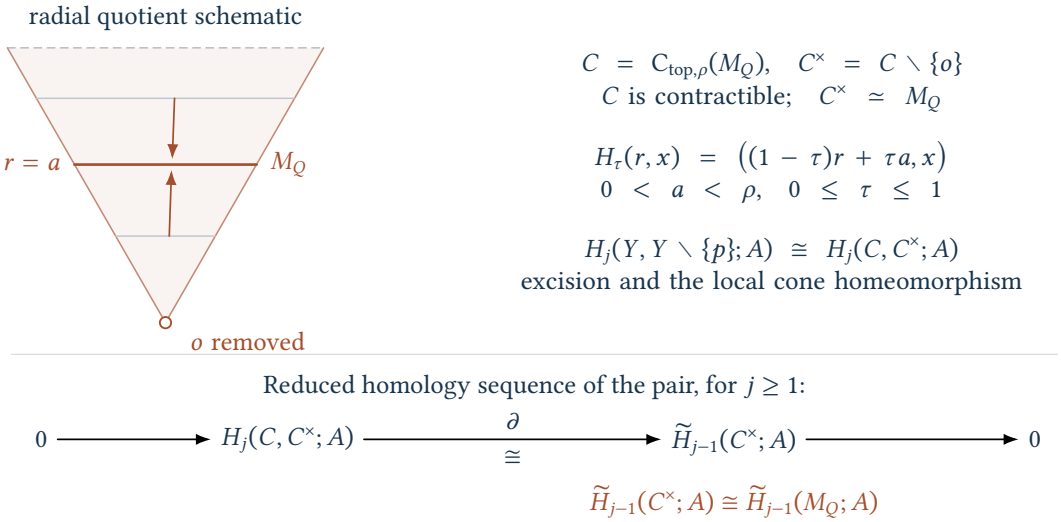



FIGURE 27. The punctured cone retracts onto $M_Q$. Contractibility of the full cone makes the connecting map in the reduced pair sequence an isomorphism for $j \geq 1$; excision identifies this with local homology in $Y$. Degree zero is handled separately in the text.

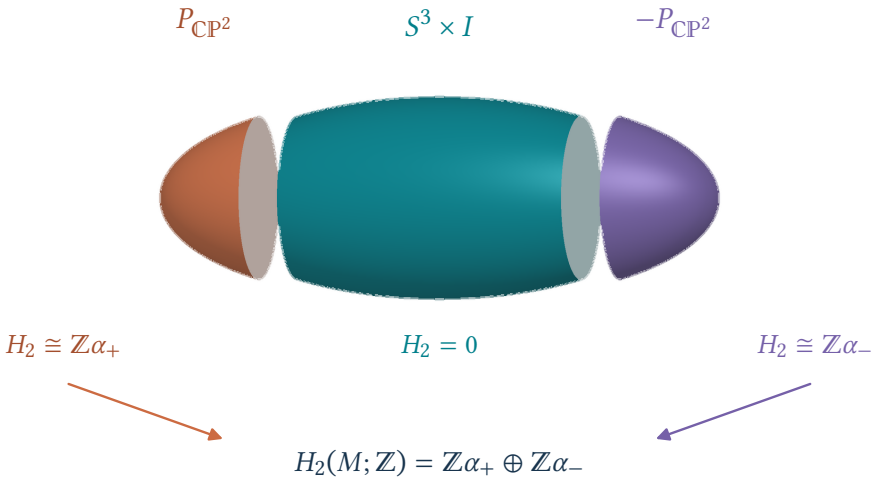



FIGURE 28. The two punctured $\mathbb{CP}^2$ cores contribute independent second-homology classes. The intervening cylinder and its boundary spheres have the vanishing groups needed in Mayer–Vietoris. The bodies show an abstract decomposition, not an asserted embedding or curvature model.

More generally, the shifted reduced homology in (21.1) is incompatible with a manifold point whenever $M_Q$ is not an integral homology $n$-sphere. This is a sufficient obstruction, not a claim that every core-admissible $Q$ gives a nonmanifold example. The conical neighbourhoods remain contractible and give local contractibility at $p$.

## 22. What "codimension two" means here

*Euclidean splitting and the size of the singular set are different measurements.*

Use $S^k(Y) = \{y : \text{no tangent at } y \text{ splits } \mathbb{R}^{k+1}\}$. Put $m = N - 2 = n - 1$. At $p$ the unique tangent is $\mathbb{R}^m \times \mathrm{C}(S^1_{2\pi q})$. The circle cone contains no line through its vertex: two points at radius one on such a line would have distance two, forcing circle distance $\pi$, whereas the circle's diameter is $\pi q < \pi$.

For completeness, a line through the vertex of the product must lie in $\mathbb{R}^m \times \{o\}$. At times $\pm t$, write its points as $(v_\pm, [r_\pm, x_\pm])$, of norm $t$. The factor triangle inequalities followed by Minkowski give

$$2t \le \sqrt{(|v_-| + |v_+|)^2 + (r_- + r_+)^2} \le t + t.$$

Both inequalities are equalities. Equality in Minkowski, with equal factor norms $t$, gives $r_- = r_+$. Equality in the cone triangle inequality would force circle distance $\pi$ if this common radius were positive. Therefore it is zero. An extra Euclidean splitting would give a distance-preserving map $\mathbb{R}^{m+1} \to \mathbb{R}^m$ fixing zero. The polarization identity applied to the images of the standard basis would give $m + 1$ orthonormal vectors in $\mathbb{R}^m$, a contradiction. The maximal splitting rank is exactly $m$. [N, Lemma 5.1].

It follows that

$$p \in S^{N-2}(Y) \setminus S^{N-3}(Y).$$

Every other point has Euclidean tangent. Hence $S^{N-3}(Y) = \emptyset$, and nesting gives $S^{N-4}(Y) = \emptyset$. In the nonmanifold examples the quantities are

| Quantity | Value |
|---|---|
| Maximal splitting at $p$ | $N - 2$ Euclidean directions |
| Topological singular set | $\{p\}$, of Hausdorff dimension zero |
| Hausdorff codimension of that set | $N$, not two |
| Topology of the tangent | $\mathbb{R}^N$ |
| Local topology at $p$ | Cone on $M_Q$, detected by relative local homology |

In the Cheeger–Colding convention translated in [N, §2], the prescribed codimension-four stratum is empty as well. Its complement has interior equal to $Y$, which is not a manifold. This is the specified-stratum conclusion addressed by [N, Corollary 3.4] and [CC, Conjecture 0.7]. It does not exclude removing a different closed set of codimension at least four: removing $\{p\}$ already leaves a smooth manifold. [N, Remark 3.5].

The examples exist in every $N \ge 5$: put $n = N - 1$ and choose

$$Q = \begin{cases} \mathbb{CP}^{n/2}, & n \text{ even}, \\ S^{n-2} \times S^2, & n \text{ odd}. \end{cases}$$

Core-admissibility is the external core-metric input applied in [N, proof of Corollary 3.3]. For even $n$, the projective cells give $H_2(Q; \mathbb{Z}) = \mathbb{Z}$; for odd $n \ge 5$, Künneth gives the same group since $n - 2 \ge 3$. Removing a disc preserves $H_2$ because the relative groups in degrees two and three vanish for $n \ge 4$. Mayer–Vietoris then gives $H_2(Q\#(-Q); \mathbb{Z}) = \mathbb{Z}^2$. The local obstruction stays in degree three while the ambient dimension increases.

## 23. A guide back to the technical proof

*Each estimate has a specific use in the next stage.*

The conceptual route is given near the beginning in Section 2. The table below locates the substantive connections developed in this revision. The reference numbers are those of the supplied 94-page manuscript [N].

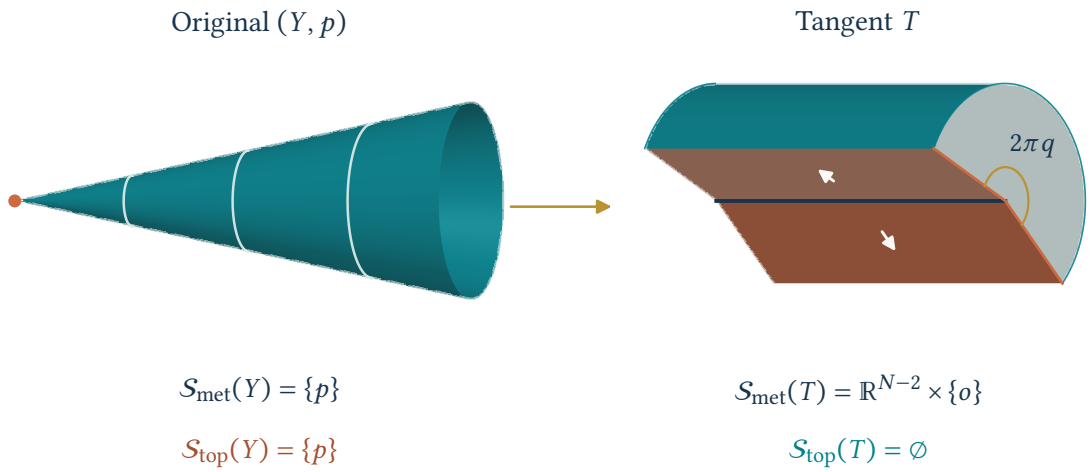



FIGURE 29. In the nonmanifold examples the original $Y$ has one metric and topological singular point. Its unique tangent is topologically $\mathbb{R}^N$, with metric singular axis $\mathbb{R}^{N-2} \times \{o\}$. The drawing shows one Euclidean factor. Here $\mathcal{S}_{\mathrm{met}}$ means points with no Euclidean tangent.

| Question | Required mechanism | Main source |
|---|---|---|
| Why this smooth link path? | Actual edge profile, curvature operator, distance estimate, exact-volume interpolation | Lemma 5.2; Theorem 5.3 |
| Why the prescribed cap boundary? | Moser in the interpolation parameter and inverse terminal collar pullback | Theorem 7.5; Proposition 7.6 |
| Why uniform cap estimates? | Path slowdown, smooth inner cut, intrinsic collar bounds, final homothety | Proposition 7.6 |
| Why does gluing work? | Boundary tensor equality, strict sums of forms, successive widths | Propositions 7.2–7.4 |
| Why exact normalized Ricci? | Relative volume surplus dominates both curvature and volume errors | Theorem 8.1 |
| Why a closable start? | Fixed symmetric seed, compact filling, exact conical attachment, scaling order | Theorem 8.1 |
| Why radial Ricci nonnegative? | Common volume form, slow parameter, full block estimates | Proposition 6.2; Lemma 9.1 |
| Why unique tangent? | Annular tensor comparison, ambient shortcuts, pointed ball correspondence | Proposition 9.2 |
| Why smooth realization? | Return to the seed, moment-preserving warp, intrinsic filling size, exact collar | Proposition 9.2 |
| Why no manifold chart? | Conical neighbourhood, punctured retraction, relative homology | §§10–11 |

The construction keeps four distinctions throughout: the fixed topological link versus the metric limit link; total volume versus volume form; diagonal Ricci components versus the full quadratic form; and small boundary size versus intrinsic diameter of a filling. The new explanations specify where each distinction enters the proof. In particular, one passes to the metric limit to identify the tangent, but computes the punctured-neighbourhood topology on the fixed manifold. These operations are not interchangeable.

## References

[N] A. Nifa, *Topological singularities in the codimension-two stratum of noncollapsed Ricci limits*, preprint, 31 July 2026. doi:10.5281/zenodo.23049912.

[CC] J. Cheeger and T. H. Colding, *On the structure of spaces with Ricci curvature bounded below. I*, J. Differential Geom. **46** (1997), 406–480. doi:10.4310/jdg/1214459974.

[CN] T. H. Colding and A. Naber, *Characterization of tangent cones of noncollapsed limits with lower Ricci bounds and applications*, Geom. Funct. Anal. **23** (2013), 134–148. arXiv:1108.3244.

[DPG] G. De Philippis and N. Gigli, *Non-collapsed spaces with Ricci curvature bounded from below*, J. Éc. polytech. Math. **5** (2018), 613–650. doi:10.5802/jep.80.

[KM] V. Kapovitch and A. Mondino, *On the topology and the boundary of $N$-dimensional* RCD$(K, N)$ *spaces*, Geom. Topol. **25** (2021), 445–495. arXiv:1907.02614.

[M] J. Moser, *On the volume elements on a manifold*, Trans. Amer. Math. Soc. **120** (1965), 286–294. doi:10.1090/S0002-9947-1965-0182927-5.

[R] P. Reiser, *Examples of tangent cones of non-collapsed Ricci limit spaces*, Nonlinear Anal. **252** (2025), Article 113699. arXiv:2409.11954.

Toulouse, France
*Email address*: nifa.anass@gmail.com